DOI: 10.1021/ic901012w

Inorganic Chemistry
Article

Synthesis and Coordination Properties of Quinoline Pendant Arm Derivatives of [9]aneN$_3$ and [9]aneN$_2$S as Fluorescent Zinc Sensors

Marta Mameli,[†] M. Carla Aragoni,[†] Massimiliano Arca,[†] Marta Atzori,[†] Andrea Bencini,[‡] Carla Bazzicalupi,[‡] Alexander J. Blake,[§] Claudia Caltagirone,[†] Francesco A. Devillanova,[†] Alessandra Garau,[†] Michael B. Hursthouse,[∥] Francesco Isaia,[†] Vito Lippolis,*[,†] and Barbara Valtancoli[‡]

[†] *Dipartimento di Chimica Inorganica ed Analitica, S.S. 554 Bivio per Sestu, Università degli Studi di Cagliari, 09042 Monserrato (CA), Italy,* [‡] *Dipartimento di Chimica, Via della Lastruccia 3, Università degli Studi di Firenze, 50019 Sesto Fiorentino (FI), Italy,* [§] *School of Chemistry, The University of Nottingham, University Park, Nottingham NG7 2RD, U.K., and* [∥] *School of Chemistry, University of Southampton, Highfield, Southampton SO17 1BJ, U.K.*

Received May 26, 2009

The coordination chemistry of three new quinoline pendant arm derivatives of [9]aneN$_3$ (**L^1**, **L^2**) and [9]aneN$_2$S (**L^3**) toward Cu^{II}, Zn^{II}, Cd^{II}, Hg^{II}, and Pb^{II} has been investigated both in solution and in the solid state. The protonation constants for **L^1**−**L^3** and stability constants with the aforementioned metal ions have been determined potentiometrically in 0.10 M NMe$_4$Cl MeCN/H$_2$O (1:1 v/v) solution at 298.1 ± 0.1 K; the measured values show that Cu^{II} has the highest affinity for all three ligands, followed by Zn^{II}, Hg^{II}, Pb^{II}, and Cd^{II}. For each metal ion considered, 1:1 complexes with **L^1**−**L^3** have also been isolated in the solid state and [Cu(**L^1**)](BF$_4$)$_2$ (**1**), [Zn(**L^1**)](BF$_4$)$_2$ (**2**), [Cd(**L^1**)](ClO$_4$)$_2$ (**3**), [Hg(**L^1**)](NO$_3$)$_2$ (**4**), [Pb(**L^1**)](ClO$_4$)$_2$·MeCN (**5**), [Zn$_2$Cl$_2$(**L^2**)$_2$](BF$_4$)$_2$·$^1/_2$MeNO$_2$·H$_2$O (**6**), [Cu(**L^3**)](ClO$_4$)$_2$ (**7**), [Zn(**L^3**)(NO$_3$)]NO$_3$ (**8**), [Cd(**L^3**)(NO$_3$)$_{0.82}$Cl$_{0.18}$]NO$_3$ (**9**), and [Hg(**L^3**)](ClO$_4$)$_2$·MeCN (**10**) have also been characterized by X-ray crystallography. The optical response of **L^1**−**L^3** to the presence of the above-mentioned metal ions has been investigated in MeCN/H$_2$O (1:1 v/v) and H$_2$O solutions. All three ligands show a stronger "OFF-ON" CHEF (chelation enhancement of fluorescence) effect in the Zn^{II} complexes than in the Cd^{II} complexes in both media. The results have been examined by considering the ratio $I_{rel}(Zn^{II})/I_{rel}(Cd^{II})$, within the emerging idea that the relative strength of the CHEF effect for the small Zn^{II} ion as compared to larger Cd^{II} ion might be determined by steric crowding in the corresponding complexes with quinoline-based fluorescent chemosensors.

Introduction

The design and synthesis of fluorescent molecular sensors that selectively and specifically respond to the presence of a given analyte (in particular metal ions) in a complex matrix is a vigorous research area of supramolecular chemistry.[1−14] Applications can span from process control to environmental monitoring, food analysis, and medical diagnosis, to give just some examples.

Chemosensors based on fluorescence offer many advantages over other types of chemosensor in terms of sensitivity, response time, and cost; they are of crucial importance for the development of detection and quantification methodologies for metal ions such as Zn^{II},[15,16] Cd^{II},[17−19] Pb^{II},[20−22], and Hg^{II}[23,24] which possess a closed-shell d^{10} configuration and,

*To whom correspondence should be addressed. E-mail: lippolis@unica.it. Phone: + 070 6754467. Fax + 070 675 4456.

(1) *Chemosensors of Ions and Molecular Recognition*; Czarnik, A. W., Desvergene, J.-P., Eds.; NATO ASI Ser., Ser. C; Kluwer Academic Publishers : Dordrecht, 1997; Vol. *492*.
(2) de Silva, A. P.; Gunaratne, H. Q. G.; Gunnlaugsson, T.; Huxley, A. J. M.; McCoy, C. P.; Rademacher, J. T.; Rice, T. E. *Chem. Rev.* **1997**, *97*, 1515.
(3) (a) Fabbrizzi, L.; Licchelli, M.; Taglietti, A. *Dalton Trans.* **2003**, 3471. (b) Amendola, V.; Fabbrizzi, L.; Foti, F.; Licchelli, M.; Mangano, C.; Pallavicini, P.; Poggi, A.; Sacchi, D.; Taglietti, A. *Coord. Chem. Rev.* **2006**, *250*, 273.
(4) Kimura, E.; Koike, T. *Chem. Soc. Rev.* **1998**, *27*, 179.
(5) Prodi, L. *New. J. Chem.* **2005**, *29*, 20.
(6) Prodi, L.; Bolletta, F.; Montalti, M.; Zaccheroni, N. *Coord. Chem. Rev.* **2000**, *205*, 59.
(7) Rurack, K. *Spectrochim. Acta, Part A* **2001**, *57*, 2161.
(8) *J. Mater. Chem.*, **2005**, *15*, 2617−2976. Theme Issue: Fluorescent Sensors.
(9) (a) Valeur, B.; Leray, I. *Coord. Chem. Rev.* **2000**, *205*, 3. (b) Métivier, R.; Leray, I.; Valeur, B. *Chem. Commun.* **2003**, 996.
(10) Martínez-Máñez, R.; Sancenón, F. *Chem. Rev.* **2003**, *103*, 4419.
(11) Kim, J. S.; Quang, D. T. *Chem. Rev.* **2007**, *207*, 3780.
(12) Basabe-Desmontes, L.; Reinhoudt, D. N.; Crego-Calama, M. *Chem. Soc. Rev.* **2007**, *36*, 993.
(13) Pallavicini, P.; Pasotti, L.; Patroni, S. *Dalton Trans.* **2007**, 5670.
(14) Lodeiro, C.; Pina, F. *Coord. Chem. Rev.* **2009**, *253*, 1353.
(15) Nolan, E. M.; Lippard, S. J. *Acc. Chem. Res.* **2009**, *42*, 193.
(16) Dai, Z.; Canary, J. W. *New J. Chem.* **2007**, *31*, 1708.
(17) Taki, M.; Desaki, M.; Ojida, A.; Iyoshi, S.; Hirayama, T.; Hamachi, I.; Yamamoto, Y. *J. Am. Chem. Soc.* **2008**, *130*, 12564.
(18) Cheng, T.; Xu, Y.; Zhang, S.; Zhu, W.; Quian, X.; Duan, L. *J. Am. Chem. Soc.* **2008**, *130*, 16160.
(19) Peng, X.; Du, J.; Fan, J.; Wang, J.; Wu, Y.; Zhao, J.; Sun, S.; Xu, T. *J. Am. Chem. Soc.* **2007**, *129*, 1500.
(20) Buie, N. B.; Talanov, V. S.; Butcher, R. J.; Talanova, G. G. *Inorg. Chem.* **2008**, *47*, 3549.
(21) He, Q.; Miller, E. W.; Wong, A. P.; Chang, C. J. *J. Am. Chem. Soc.* **2006**, *128*, 9316.
(22) Roussakis, E.; Pergantis, S. A.; Katerinopoulos, H. E. *Chem. Commun.* **2008**, 6221.
(23) Nolan, E. M.; Lippard, S. J. *Chem. Rev.* **2008**, *108*, 3443.
(24) Zhao, Y.; Lim, Z.; He, C.; Wu, H.; Duan, C. *Inorg. Chem.* **2006**, *45*, 10013.

Published on Web 09/11/2009

therefore, cannot be observed through classical techniques like electronic magnetic resonances, Mössbauer and electronic absorption spectroscopies, and, in some cases, nuclear magnetic resonance spectroscopy.

The most common synthetic approach to the synthesis of fluorescent chemosensors is to link covalently, through an appropriate spacer, a fluorogenic fragment (signaling unit) to a guest-binding site (receptor unit). The recognition of the target species by the receptor unit (the result of a selective host−guest interaction between them) elicits an optical signal expressed as an enhancement or quenching of the fluorophore emission. The choice of both the signaling- and the receptor-units can be critical to both the performance and the selectivity/specificity of the sensor, especially if a direct interaction between the fluorophore and the target species is possible.

Different fluorophores (anthracene, 8-hydroxyquinoline, dansylamide, phenanthroline, etc.) are used as signaling sites,[1−14] whereas macrocyclic receptors continue to represent the first choice as guest-binding sites for metal cations because of the extensive possibilities which they can offer for modulation of the topology and nature of the binding domain, thus providing an easy route to achieving strong and possibly selective interactions with the substrate of interest. Many of the reported fluorescent chemosensors feature polyoxa-, polyaza-, and azaoxa-macrocycles as receptor units, whereas few examples are reported of fluorescent chemosensors for metal cations comprising S-donor macrocycles as the binding site.[1−14] Interestingly, apart from a few examples reported by Czarnik et al. in the early 1990s,[25] and by Yoon in 1999,[26] to our knowledge no ligands designed to be used as conjugated fluorescent chemosensors for metal ions, and featuring small macrocycles like [9]aneN$_3$ (1,4,7-triazacyclononane) and [9]aneN$_2$S (1,4-diaza-7-thiacyclononane) as receptor units, are reported.[27] This type of small macrocycle has played an important role in the development of macrocyclic coordination chemistry and continue to be of considerable interest.[28−30] In particular the binding properties of [9]aneN$_3$ and [9]aneN$_2$S can be finely tuned through sequential functionalization of the secondary amines with pendant arms bearing additional coordinating groups to generate ligands with increasing numbers of donor atoms. These often confer remarkable stability upon metal centers in low nuclearity complexes, and can adapt to the preferred coordination geometries and oxidation states of the metal center(s).[28−30] Following our interest in both the coordination chemistry and properties of [9]aneN$_3$ and [9]aneN$_2$S derivatives,[29,31−36] and the development of fluorescent molecular sensors for metal cations,[37−39] we describe here the synthesis and coordination properties of three new quinoline-based pendant arm derivatives of [9]aneN$_3$ and [9]aneN$_2$S ($\mathbf{L^1}$−$\mathbf{L^3}$ in Scheme 1) toward Cu^{II}, Zn^{II}, Cd^{II}, Hg^{II}, and Pb^{II}. Furthermore the optical responses of $\mathbf{L^1}$−$\mathbf{L^3}$ to the above-mentioned metal ions were measured as a function of pH in MeCN/H$_2$O (1:1 v/v) and H$_2$O to study the effect, in terms of substrate-specific response, of the different bonding domains and steric crowding determined by both the macrocyclic framework and the coordinating pendant arms.

Experimental Section

Instruments and Materials. All melting points are uncorrected. Microanalytical data were obtained using a Fisons EA CHNS-O instrument (T = 1000 °C). ^{1}H and ^{13}C NMR spectra were recorded on a Varian VXR300 or a Varian VXR400 spectrometer, and peak positions are reported relative to tetramethylsilane (SiMe$_4$). Electrospray Ionization (ESI) mass spectra were obtained on a MS spectrometer HP 5989A.

The spectrophotometric measurements were carried out at 25 °C using a Varian model Cary 5 UV−vis NIR spectrophotometer and a Thermo Nicolet Evolution 300 spectrophotometer. Uncorrected emission spectra were obtained with a Varian Cary Eclipse fluorescence spectrophotometer. To allow comparison among emission intensities, we performed corrections for instrumental response, inner filter effect, and phototube sensitivity.[40] A correction for differences in the refractive index and for the absorbed light was introduced when necessary.[40] Luminescence quantum yields were determined using quinine sulfate in a 1 M H$_2$SO$_4$ aqueous solution (Φ = 0.546) as a reference. For spectrophotometer measurements, MeCN (Uvasol, Merck) and Millipore grade water were used as solvents. Spectrofluorimetric titrations of the $\mathbf{L^1}$−$\mathbf{L^3}$ with metal ions were performed by adding to a solution of the ligand (3 mL), buffered at pH 7.4 with MOPS (3 μL of 1 M aqueous solution) [MOPS = 3-*N*-morpholino-propansulfonic acid], increasing volumes of a solution of the metal ion. Solutions of the ligands in MeCN/H$_2$O (1:1 v/v) or in H$_2$O were 2.5×10^{-5} M, and those of the metals in H$_2$O were 2.5×10^{-3} M. Spectrofluorimetric titrations at variable pH of $\mathbf{L^1}$−$\mathbf{L^3}$ were performed by adding to an acid solution of the ligand or its 1:1 metal ion complex in MeCN/H$_2$O (1:1 v/v,10 mL, 2.5×10^{-5} M) or in H$_2$O (2.5×10^{-5} M) in the presence of MOPS (100 μL of 1 M aqueous solution), increasing volumes of 0.5 M aqueous NaOH; the initial pH was adjusted by adding aqueous HCl (0.2 mL, 0.5 M). In all cases the effect of dilution on fluorescence emission was neglected. Solvents for other purposes and starting materials where purchased from commercial sources where available. 1,4,7-Triazacyclononane,[41] 1,4,7-triazatricyclo[5.2.1.0^{4,10}]-decane,[41] 1,4-diaza-7-thiacyclononane[42] were prepared by

(25) Akkaya, E. U.; Huston, M. E.; Czarnik, A. W. *J. Am. Chem. Soc.* **1990**, *112*, 3590.
(26) Yoon, J. *J. Ind. Eng. Chem.* **1999**, *5*, 212.
(27) Nonat, A.; Imbert, D.; Pécques, J.; Giraud, M.; Mazzanti, M. *Inorg. Chem.* **2009**, *48*, 4207.
(28) Chaudhuri, P.; Wieghardt, K. *Prog. Inorg. Chem.* **1987**, *35*, 329.
(29) Schröder, M.; Lippolis, V. In *Macrocyclic Chemistry: Current Trends and Future Perspectives*; Gloe, K., Ed.; Springer: The Netherlands, 2005.
(30) Danks, J. P.; Champness, N. R.; Schröder, M. *Coord. Chem. Rev.* **1998**, *174*, 417.
(31) Lippolis, V.; Blake, A. J.; Cooke, P. A.; Isaia, F.; Li, W.-S.; Schröder, M. *Chem.—A Eur. J.* **1999**, *5*, 1987.
(32) Arca, M.; Blake, A. J.; Lippolis, V.; Montesu, D. R.; McMaster, J.; Tei, L.; Schröder, M. *Eur. J. Inorg. Chem.* **2003**, 1232.
(33) Shamsipur, M.; Poursaberi, T.; Rezapour, M.; Ganjali, M. R.; Mousavi, M. F.; Lippolis, V.; Montesu, D. R. *Electroanalysis* **2004**, *16*, 1336.
(34) Arca, M.; Bencini, A.; Berni, E.; Caltagirone, C.; Devillanova, F. A.; Isaia, F.; Garau, A.; Giorgi, C.; Lippolis, V.; Perra, A.; Tei, L.; Valtancoli, B. *Inorg. Chem.* **2003**, *42*, 6929.
(35) Bazzicalupi, C.; Bencini, A.; Faggi, E.; Garau, A.; Giorgi, V.; Lippolis, V.; Perra, A.; Valtancoli, B. *Dalton Trans.* **2006**, 1409.
(36) Arturoni, E.; Bencini, A.; Caltagirone, C.; Danesi, A.; Garau, A.; Giorgi, C.; Lippolis, V.; Valtancoli, B. *Inorg. Chem.* **2008**, *47*, 6551.
(37) Blake, A. J.; Bencini, A.; Caltagirone, C.; De Filippo, G.; Dolci, L. S.; Garau, A.; Isaia, F.; Lippolis, V.; Mariani, P.; Prodi, L.; Montalti, M.; Zaccheroni, N.; Wilson, C. *Dalton Trans.* **2004**, 2771.
(38) Aragoni, M. A.; Arca, M.; Bencini, A.; Blake, A. J.; Caltagirone, C.; De Filippo, G.; Devillanova, F. A.; Garau, A.; Gelbrich, T.; Hursthouse, M. B.; Isaia, F.; Lippolis, V.; Mameli, M.; Mariani, P.; Valtancoli, B.; Wilson, C. *Inorg. Chem.* **2007**, *46*, 4548.
(39) Aragoni, M. A.; Arca, M.; Bencini, A.; Blake, A. J.; Caltagirone, C.; Danesi, A.; Devillanova, F. A.; Garau, A.; Gelbrich, T.; Isaia, F.; Lippolis; Hursthouse, M. B.; Valtancoli, B.; Wilson, C. *Inorg. Chem.* **2007**, *46*, 8088.
(40) Credi, A.; Prodi, L. *Spectrochim. Acta* **1998**, *54*, 159.
(41) Atkins, T. J. *J. Am. Chem. Soc.* **1980**, *102*, 6363.
(42) Blake, A. J.; Danks, J. P.; Harrison, A.; Parsons, S.; Schooler, P.; Whittaker, G.; Schröder, M. *J. Chem. Soc., Dalton Trans.* **1998**, 2335.

Scheme 1. Ligands Considered in This Paper

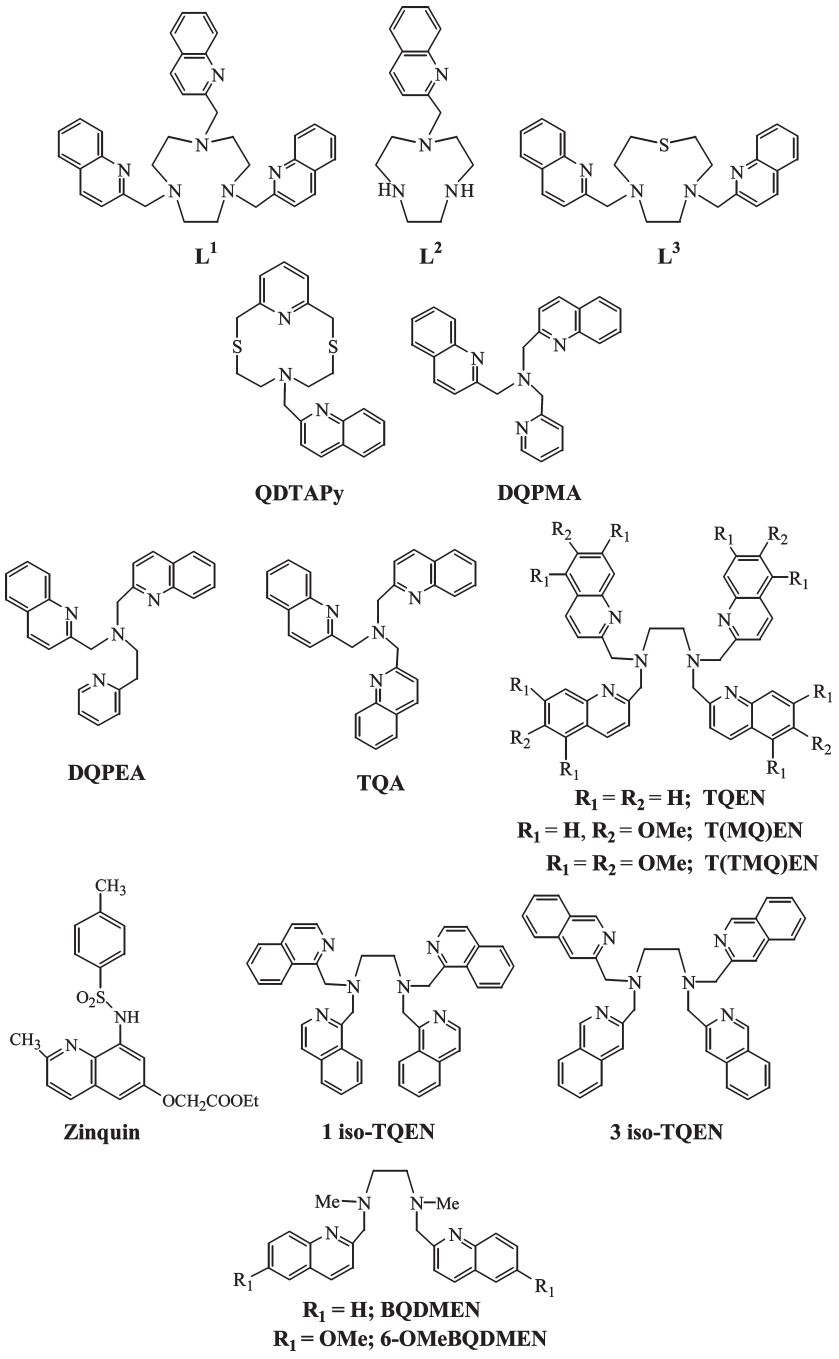

published methods. Synthetic details including analytical data for $\mathbf{L^1}$−$\mathbf{L^3}$ have been deposited as Supporting Information.

Caution! *Some of the reported metal complexes were isolated in the solid state as perchlorate salts. We have worked extensively with these complexes on a small scale without any incident. Despite these observations, the unpredictable behavior of perchlorate salts necessitates extreme care in handling.*

Synthesis of Metal Complexes. 1:1 metal complexes of $\mathbf{L^1}$−$\mathbf{L^3}$ with Cu^{II}, Zn^{II}, Cd^{II}, Pb^{II}, and Hg^{II} have been synthesized by following a standard procedure which involves the mixing of the appropriate metal salt and the ligand ($\mathbf{L^1}$, $\mathbf{L^2}$, or $\mathbf{L^3}$) in 1:1 molar ratio in MeCN, and the isolation of the product as crystals or powder from the reaction mixture stirred for a few hours at room temperature, by diffusion of Et_2O vapors or by evaporation of the solvent. Synthetic details including analytical data for the isolated complexes have been deposited as Supporting Information.

Potentiometric Measurements. All pH measurements (pH = −log [H^+]) employed for the determination of ligand protonation and metal complex stability constants were carried out in 0.10 M NMe_4Cl MeCN/H_2O (1:1 v/v) solution at 298.1 ± 0.1 K by means of conventional titration experiments under an inert atmosphere. The choice of solvent mixture was dictated by the low solubility of the ligand in pure water. The equipment and procedure used has been previously described.[43] The standard potential E° and the ionic product of water (pK_w = 14.99(1) at 298.1 ± 0.1 K in 0.10 M NMe_4Cl) were determined by Gran′s method.[44] At least three measurements (with about 100 data points for each) were performed for each system in the pH

(43) Bencini, A.; Bianchi, A.; Micheloni, M.; Paoletti, P.; Garcia-España, E.; Nino, M. A. *J. Chem. Soc., Dalton Trans.* **1991**, 1171.
(44) Gran, G. *Analyst* (*London*) **1952**, *77*, 661.

Table 1. Crystallographic Data for $[Cu(\mathbf{L^1})](BF_4)_2$ (**1**), $[Zn(\mathbf{L^1})](BF_4)_2$ (**2**), $[Cd(\mathbf{L^1})](ClO_4)_2$ (**3**), $[Hg(\mathbf{L^1})](NO_3)_2$ (**4**), and $[Pb(\mathbf{L^1})](ClO_4)_2 \cdot MeCN$ (**5**)

	1	**2**	**3**	**4**	**5**
formula	$C_{36}H_{36}B_2CuF_8N_6$	$C_{36}H_{36}B_2F_8N_6Zn$	$C_{36}H_{36}CdCl_2N_6O_8$	$C_{36}H_{36}HgN_8O_6$	$C_{38}H_{39}Cl_2N_7O_8Pb$
crystal system	triclinic	triclinic	triclinic	monoclinic	triclinic
space group	$P\bar{1}$	$P\bar{1}$	$P\bar{1}$	$P2_1/c$	$P\bar{1}$
MW	789.87	791.70	864.01	877.32	999.85
a/Å	12.230(1)	12.1942(13)	11.7914(7)	16.931(2)	10.365(1)
b/Å	12.329(1)	12.5107(13)	12.222(1)	14.016(2)	10.980(1)
c/Å	13.398(2)	13.1203(14)	14.241(1)	14.825(2)	20.099(2)
α/deg	72.44(1)	73.026(2)	71.382(7)		89.962(9)
β/deg	79.33(1)	79.848(2)	78.563(5)	92.350(10)	104.557(9)
γ/deg	64.77(1)	62.756(2)	70.959(6)		116.83(1)
V/Å^3	1738.6(3)	1699.9(3)	1828.3(2)	3515.1(8)	1958.7(3)
Z	2	2	2	4	2
T/K	298	150(2)	298	298	298
D_c/g cm^{-3}	1.509	1.547	1.569	1.658	1.695
μ mm^{-1}	0.709	0.805	0.804	4.437	4.504
unique reflections, R_{int}	7772, 0.039	7616, 0.014	6625, 0.074	5951, 0.079	7508, 0.047
observed reflections [$I > 2\sigma(I)$]	4496	6728	4042	3000	5814
Absorption correction	SCALE3 ABSPACK[47]	SADABS[48]	SCALE3 ABSPACK[47]	SCALE3 ABSPACK[47]	SCALE3 ABSPACK[47]
T_{min}, T_{max}	0.750, 0.780	0.860, 1.000	0.666, 0.923	0.355, 0.642	0.349, 0.637
R_1	0.0639	0.0329	0.0606	0.0400	0.0405
wR_2 [all data]	0.1890	0.0892	0.1577	0.0692	0.0915

Table 2. Crystallographic Data for $[Zn_2Cl_2(\mathbf{L^2})_2](BF_4)_2 \cdot {}^1/_2MeNO_2 \cdot H_2O$ (**6**), $[Cu(\mathbf{L^3})](ClO_4)_2$ (**7**), $[Zn(\mathbf{L^3})(NO_3)]NO_3$ (**8**), $[Cd(\mathbf{L^3})(NO_3)_{0.82}Cl_{0.18}]NO_3$ (**9**), and $[Hg(\mathbf{L^3})](ClO_4)_2 \cdot MeCN$ (**10**)

	6	**7**	**8**	**9**	**10**
formula	$C_{32.5}H_{47.5}B_2Cl_2F_8N_{8.5}O_2Zn_2$	$C_{26}H_{28}Cl_2CuN_4O_8S$	$C_{26}H_{28}N_6O_6SZn$	$C_{26}H_{28}CdCl_{0.18}N_{5.82}O_{5.46}S$	$C_{28}H_{31}Cl_2HgN_5O_8S$
crystal system	triclinic	monoclinic	triclinic	triclinic	Orthorhombic
space group	$P\bar{1}$	$P2_1/c$	$P\bar{1}$	$P\bar{1}$	$Pbca$
MW	964.55	691.02	617.97	660.24	869.13
a/Å	8.2373(17)	16.0459(4)	11.1654(3)	7.6141(2)	9.7286(3)
b/Å	11.154(2)	13.4132(2)	15.2985(4)	13.1464(7)	17.2483(5)
c/Å	12.383(3)	14.1302(4)	15.5541(4)	14.5730(8)	36.4320(11)
α/deg	102.531(3)		88.799(2)	98.771(2)	
β/deg	100.898(3)	111.205(1)	83.436(2)	93.626(3)	
γ/deg	101.839(3)		89.750(2)	93.998(3)	
V/Å^3	1054.0(4)	2835.29(11)	2638.85(12)	1434.12(12)	6113.4(3)
Z	1	4	4	2	8
T/K	150(2)	120(2)	120(2)	120(2)	120(2)
D_c/g cm^{-3}	1.520	1.619	1.555	1.529	1.889
μ mm^{-1}	1.341	1.090	1.064	0.898	5.337
unique reflections, R_{int}	3675, 0.033	6503, 0.084	11822, 0.072	6546, 0.093	6940, 0.052
observed reflections [$I > 2\sigma(I)$]	3014	4739	9675	4741	5827
absorption correction	SADABS[48]	SADABS[48]	SADABS[48]	SADABS[48]	SADABS[48]
T_{min}, T_{max}	0.591, 1.000	0.812, 0.979	0.676, 0.883	0.933, 0.966	0.415, 0.901
R_1	0.0715	0.046	0.0771	0.0545	0.0512
wR_2 [all data]	0.2096	0.1111	0.2244	0.1259	0.1100

ranges 2−10.5. In all experiments the ligand concentration [L] was about 1×10^{-3} M. In the complexation experiments the metal ion concentration was varied from 0.5:1 to 0.9:1. The computer program HYPERQUAD[45] was used to calculate the equilibrium constants from emf data. In the case of Hg^{II}, under the experimental conditions employed, the formation of metal−chloride complexes is expected to occur. The formation of such complexes was not taken into account in calculations; hence, the stability constants of Hg^{II} complexes reported (see below) must be referred to the specific composition of the medium employed [0.10 M NMe_4Cl, $MeCN/H_2O$ (1:1 v/v)].

^{1}H NMR Titrations. The ^{1}H NMR spectra of $\mathbf{L^1}-\mathbf{L^3}$ on changing the pH were recorded on solutions of the ligands in CD_3CN/D_2O (1:1 v/v) at 298 K, by using a Bruker 400 MHz Advance spectrometer. Peak positions are relative to DSS (2,2-dimethyl-2-silapentane-5-sulfonate, sodium salt). Small amounts of 0.01 M NaOD or DCl solutions were used to adjust the pD. The pH was calculated from the measured pD values using the relationship: pH = pD − 0.40.[46]

Crystallography. A summary of the crystal data and refinement details for the compounds discussed in this paper is given in Tables 1 and 2. Only special features of the analyses are mentioned here. Single-crystal data collection for $[Zn(\mathbf{L^1})](BF_4)_2$ (**2**) and $[Zn_2Cl_2(\mathbf{L^2})_2](BF_4)_2 \cdot {}^1/_2MeNO_2 \cdot H_2O$ (**6**) was performed on a Bruker SMART APEX CCD area detector diffractometer, equipped with an Oxford Cryosystems open-flow nitrogen cryostat, using ω scans and graphite-monochromated Mo Kα radiation (λ = 0.71073 Å). The

(45) Gans, P.; Sabatini, A.; Vacca, A. *Talanta* **1996**, *43*, 1739.

(46) Covington, A. K.; Paabo, M.; Robinson, R. A.; Bates, R. G. *Anal. Chem.* **1968**, *40*, 700.

(47) *CrysAlis RED and Scale3 Abspack*, Version 1.171.32.29; Oxford Diffraction Ltd: Abingdon, Oxfordshire, U.K.

(48) Sheldrick, G. M. *SADABS Area-Detector Absorption Correction Program*; Bruker AXS Inc.: Madison, WI, 1996−2008.

data collections for $[Cu(\mathbf{L^1})](BF_4)_2$ (**1**), $[Cd(\mathbf{L^1})](ClO_4)_2$ (**3**), $[Hg(\mathbf{L^1})](NO_3)_2$ (**4**), and $[Pb(\mathbf{L^1})](ClO_4)_2 \cdot MeCN$ (**5**) were carried out with an Oxford Diffraction Xcalibur 3 CCD area detector, using ω scans and graphite-monochromated Mo Kα radiation. Finally, intensity data for $[Cu(\mathbf{L^3})](ClO_4)_2$ (**7**), $[Zn(\mathbf{L^3})(NO_3)]NO_3$ (**8**), $[Cd(\mathbf{L^3})(NO_3)_{0.82}Cl_{0.18}]NO_3$ (**9**), and $[Hg(\mathbf{L^3})](ClO_4)_2 \cdot MeCN$ (**10**) were collected, using ω scans and Mo Kα radiation, on a Bruker-Nonius Kappa CCD (**7**−**9**) or a Bruker-Nonius APEXII CCD (**10**) area-detector diffractometer mounted at the window of a rotating anode FR591 generator, and equipped with an Oxford Cryosystems open-flow nitrogen cryostat. All data sets were corrected for Lorentz, polarization, and absorption effects as specified in Tables 1 and 2. With the exception of **1** and **3**−**5**, where the structure was solved using SIR2004,[49] all the structures were solved by direct methods using SHELXS97.[50] The structures were completed by iterative cycles of full-matrix least-squares refinement and ΔF syntheses using SHELXL97.[51] All non-H atoms were refined anisotropically, except for those in the disordered groups in **6** and **9**, and H atoms were introduced at calculated positions and refined using a riding model. In **3**, one of the perchlorate counteranions was affected by disorder of two oxygen atoms, which was modeled using partial occupancy models over two sites with occupancy factors of 0.50 for each oxygen.

In **4**, both nitrate anions were found to exhibit disorder of the three oxygen atoms, and this disorder was modeled using partial occupancy models over two sites for each oxygen with occupancy factors of 0.70/0.30 for the oxygen atoms centered on N(8) and 0.50 for the oxygen atoms centered on N(9). In **6**, it was not possible to incorporate the solvent molecules in terms of discrete atomic sites; we therefore employed the SQUEEZE function in PLATON[52] to identify diffuse electron density corresponding to 25 electrons per unit cell, which we assigned to 0.5 molecules of $MeNO_2$ and one molecule of H_2O per unit cell, in good agreement with the microanalytical data. In **6**, all carbon atoms of one [9]aneN_3 moiety were found to exhibit disorder, and this disorder was modeled using partial occupancy models over two sites for each carbon with occupancy factors of 0.65/0.35. A similar modeling scheme (but with occupancy factors 0.80/0.20) was adopted for the disorder exhibited also by three of the four fluorine atoms in the BF_4^- anion in **6**. During the refinement, appropriate restraints were applied to the C−C and B−F distances, and to the F−B−F angles. For **7**, one of the perchlorate ions was disordered such that two "*trans*" orientations shared one O_3 face. In **9**, the observation of an unusually low value for the displacement parameter for the N-atom of the coordinated nitrate ion, coupled with high values for these parameters of the nitrate O-atoms, led to the recognition that the site was partially occupied by a chloride anion. Subsequent refinement using this model indicated the presence of NO_3^- and Cl^- (presumably deriving from impurities in the starting materials) in the ratio 0.82/0.18. The atoms of the high-occupancy nitrate were refined with anisotropic displacement parameters, while the low-occupancy chloride was refined with an isotropic displacement parameter.

Results and Discussion

Synthesis and Protonation of $\mathbf{L^1}$−$\mathbf{L^3}$. $\mathbf{L^1}$ and $\mathbf{L^3}$ were prepared easily in reasonable yields by reacting [9]aneN_3 and [9]aneN_2S with 3 and 2 equiv of 2-(chloromethyl)-quinoline, respectively, in toluene and in the presence of KOH (see Supporting Information). As regards the synthesis of $\mathbf{L^2}$, selective *N*-functionalization of [9]aneN_3 with only one or two pendant arms using a multistep approach is more difficult to achieve than symmetric *N*-functionalization. The most successful synthetic procedures for the monofunctionalization of [9]aneN_3 feature the use of appropriate protecting groups for two of the three nitrogen atoms of the macrocyclic ligand.[28,29] A very versatile starting material for the asymmetric monofunctionalization of [9]aneN_3 is its tricyclic orthoamide derivative 1,4,7-triazatricyclo[5.2.1.$0^{4,10}$]decane (HC[9]aneN_3).[41] Indeed, the reaction of HC[9]aneN_3 with 1 equiv of 2-(chloromethyl)quinoline in MeCN afforded, after base hydrolysis of the amidinium salt intermediate, a quantitative yield of $\mathbf{L^2}$ (see Supporting Information).

Table 3. Protonation Constants (log *K*) of $\mathbf{L^1}$, $\mathbf{L^2}$, and $\mathbf{L^3}$[a]

reaction	log *K*		
	$\mathbf{L^1}$	$\mathbf{L^2}$	$\mathbf{L^3}$
$L + H^+ \rightleftharpoons (HL)^+$	9.94(4)	9.8(1)	10.04 (8)
$(HL)^+ + H^+ \rightleftharpoons (H_2L)^{2+}$	4.07(7)	6.7(1)	4.22(9)
$(H_2L)^{2+} + H^+ \rightleftharpoons (H_3L)^{3+}$	2.99(7)	3.1(1)	
$(H_3L)^{3+} + H^+ \rightleftharpoons (H_4L)^{4+}$	1.8(1)		

[a] MeCN/H_2O (1:1 v/v), 0.10 M NMe_4Cl, 298.1 K.

The protonation behavior of $\mathbf{L^1}$−$\mathbf{L^3}$ was studied by means of potentiometric measurements at 298.1 K, using MeCN/H_2O (1:1 v/v) as solvent because of the low solubility of all these ligands in pure H_2O. In solution $\mathbf{L^1}$, $\mathbf{L^2}$, and $\mathbf{L^3}$ bind up to four, three, and two protons, respectively (Table 3). As often found for small macrocyclic polyamines,[53] the value of the first protonation constant (ca. 10 log units) is rather high and accounts for the protonation of an aliphatic amine group of the macrocyclic framework; in the resulting $(HL)^+$ species the acidic proton is likely to be enclosed within the macrocyclic cavity, stabilized by a hydrogen bonding network involving the other nitrogen donors. The remaining protonation steps take place at acidic pH values. Accordingly, the data in Table 3 clearly show that all three ligands $\mathbf{L^1}$−$\mathbf{L^3}$ behave as rather strong bases in the addition of the first proton. The observed higher value of the second protonation constant for $\mathbf{L^2}$ can be attributed to the protonation of a secondary amine group, which is more basic than a tertiary one of $\mathbf{L^1}$ or $\mathbf{L^3}$. However, the log *K* values for the second protonation constant of $\mathbf{L^1}$ and $\mathbf{L^3}$, and the third one for $\mathbf{L^2}$, are even lower than that reported for quinoline (log $K = 4.94$),[54] and therefore the corresponding protonation steps as well as the third and fourth ones for $\mathbf{L^1}$ could occur either on a tertiary amine donor or on a quinoline nitrogen. Further information on the protonation behavior of the ligands can be obtained by recording ^{1}H NMR spectra at different pH values and comparing the observed shifts of the signals with the distribution diagrams of the different protonated species. $\mathbf{L^1}$ exhibits two sharp singlets for the aliphatic portion of the molecule, attributable to the methylene groups of the [9]aneN_3 framework and to the methylene groups

(49) Burla, M. C.; Caliandro, R.; Cavalli, M.; Carrozzini, B.; Cascarano, G. L.; Giacovazzo, C.; Polidori, G.; Spagna, R. *J. Appl. Crystallogr.* **2005**, *38*, 381.
(50) *SHELXS*86−97; Sheldrick, G. M. *Acta Crystallogr., Sect. A* **1990**, *46*, 467.
(51) *SHELXL*97; Sheldrick, G. M. *Acta Crystallogr., Sect. A* **2008**, *64*, 112.
(52) Spek, A. L. *J. Appl. Crystallogr.* **2003**, *36*, 7.
(53) Bencini, A.; Bianchi, A.; Garcia-España, E.; Micheloni, M.; Ramirez, J. A. *Coord. Chem. Rev.* **1999**, *188*, 97.
(54) Schulman, S. G.; Capomacchina, A. C. *J. Am. Chem. Soc.* **1973**, *95*, 2763.

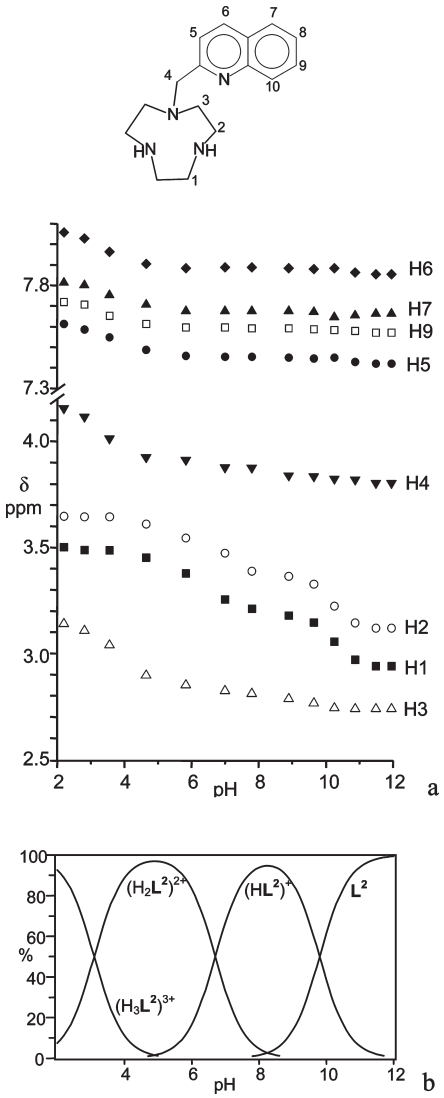

Figure 1. (a) pH-dependence of the ^{1}H NMR signals of $\mathbf{L^2}$ (the signals of the protons H8 and H10 do not shift significantly over the pH range investigated and their chemical shifts are omitted for clarity) (CD_3CN/D_2O, 1:1 v/v, 298.1 K, 0.10 M NMe_4Cl). (b) Distribution diagram of the protonated species of $\mathbf{L^2}$ (MeCN/H_2O, 1:1 v/v, 298.1 K, 0.10 M NMe_4Cl).

connecting the macrocycle to the quinoline moieties, and six signals for the aromatic protons of quinoline (C_{3v} time-averaged symmetry in solution). $\mathbf{L^2}$ and $\mathbf{L^3}$ feature four ^{1}H NMR signals for the aliphatic protons and six for the heteroaromatic hydrogens (C_{2v} time-averaged symmetry in solution). As shown in Figure 1 for $\mathbf{L^2}$, the formation in the pH range 11−5 of the mono- and diprotonated species of the ligand, $(H\mathbf{L^2})^+$ and $(H_2\mathbf{L^2})^{2+}$, is accompanied by a marked downfield shift of the ^{1}H NMR signals of the methylene groups H1 and H2 adjacent to the secondary amine groups. Minor shifts are observed for the signals of H3 and H4, adjacent to the tertiary amine group as well as for resonances of quinoline. These data support the hypothesis that the acidic protons in $(H\mathbf{L^2})^+$ and $(H_2\mathbf{L^2})^{2+}$ are mainly localized on the secondary nitrogens. Conversely, the formation of the species $(H_3\mathbf{L^2})^{3+}$ below pH 5 gives rise to a noticeable downfield shift of the signals of the aliphatic protons H3 and H4 and of the heteroaromatic protons H5, H6, H7, and H9. This strongly suggests that binding of the third acidic proton involves both the aliphatic tertiary amine group and the nitrogen of quinoline, i.e., the acidic proton can be exchanged rapidly between these two nitrogen atoms and/or shared via hydrogen bonding. $\mathbf{L^1}$ and $\mathbf{L^3}$ display a similar behavior. In fact, remarkable downfield shifts are observed for the signals of the aliphatic protons upon the formation of $(H\mathbf{L})^+$ and $(H_2\mathbf{L})^{2+}$ ($\mathbf{L}$ = $\mathbf{L^1}$ or $\mathbf{L^3}$), indicating that the first and second acidic protons are essentially located on the aliphatic tertiary amine groups (Supporting Information, Figures S1 and S2). However, no negligible downfield shifts are observed for most of the signals of the quinoline protons either, suggesting the presence of hydrogen bonding interactions between the protonated aliphatic ammonium group(s) and the heteroaromatic nitrogens and/or a partial localization of the acidic protons on the nitrogens of the quinoline units. In the case of $\mathbf{L^1}$, a more marked downfield shift of the resonances of the quinoline protons is observed below pH 4, with the formation of the species $(H_3\mathbf{L^1})^{3+}$; at the same time, the signals of the aliphatic protons of $\mathbf{L^1}$ (H1 and H2 in Supporting Information, Figure S1) do not shift appreciably for pH values lower than 4. This could indicate that the third protonation step takes place on a heteroaromatic nitrogen atom (Supporting Information, Figure S1).

Metal Complexation: Solution Studies. Considering metal complexation of $\mathbf{L^1}$−$\mathbf{L^3}$ with Cu^{II}, Zn^{II}, Cd^{II}, Hg^{II}, and Pb^{II}, the potentiometric study in MeCN/H_2O (1:1 v/v) was limited at the acidic pH region because the complexes precipitate from solution at neutral pH values. Nevertheless, all three ligands form stable 1:1 complexes at acidic pH values (Supporting Information, Figures S3−S5), and therefore, the relevant stability constants of the complexes $[M(\mathbf{L})]^{2+}$ ($\mathbf{L}$ = $\mathbf{L^1}$−$\mathbf{L^3}$) could be determined in all cases, with the exception of the complexes $[Hg(\mathbf{L^2})]^{2+}$ and $[Cu(\mathbf{L})]^{2+}$ ($\mathbf{L}$ = $\mathbf{L^1}$ and $\mathbf{L^3}$; Table 4). The 1:1 Cu^{II} complexes with $\mathbf{L^1}$ and $\mathbf{L^3}$ are in fact completely formed in all the pH range investigated, even at pH 2, and their log K values can be only estimated as higher than 17. The stability of the 1:1 Hg^{II} complex with $\mathbf{L^2}$, in contrast, could not be determined because of its low solubility even in the acidic pH region. Finally, in the case of $\mathbf{L^1}$ complexation with Cd^{II} and Pb^{II} and of $\mathbf{L^2}$ complexation with Zn^{II}, the formation of $[M(H\mathbf{L})]^{3+}$ monoprotonated species is also detected below pH 5 (Supporting Information, Figures S3 and S4).

The stability constants of the 1:1 complexes of $\mathbf{L^1}$−$\mathbf{L^3}$ with these metal cations are remarkably higher (in most cases by 3 orders of magnitude or more) than those of the corresponding complexes of [9]aneN_3 and [9]aneN_2S, determined in aqueous solutions.[55] This difference is too high to be solely due to the different medium used in our measurements and may be attributed to the involvement of the quinoline nitrogen donors in metal coordination.

As generally observed with polyamine ligands, Cu^{II} forms the most stable complexes with $\mathbf{L^1}$−$\mathbf{L^3}$, because of

(55) For L = [9]aneN_3: $[Cu(L)]^{2+}$, log K = 15.5; $[Zn(L)]^{2+}$, log K = 11.6; $[Cd(L)]^{2+}$, log K = 9.4; $[Pb(L)]^{2+}$, log K = 6.76. For L = [9]aneN_2S: $[Cu(L)]^{2+}$, log K = 12.42; $[Zn(L)]^{2+}$, log K = 7.31; $[Cd(L)]^{2+}$, log K = 6.65; $[Pb(L)]^{2+}$, log K = 11.0. Values taken from: Hancock, R. D.; Dobson, S. M.; Boeyens, J. C. A. *Inorg. Chim. Acta* **1987**, *133*, 221.

Table 4. Formation Constants (log *K*) of the Metal Complexes with $\mathbf{L^1}-\mathbf{L^3}$[a]

reaction	log *K*				
	Cu^{II} [b]	Zn^{II} [b]	Cd^{II} [b]	Pb^{II} [b]	Hg^{II} [b,c]
$M^{2+} + \mathbf{L^1} \rightleftharpoons [M(\mathbf{L^1})]^{2+}$	> 17	14.2(1)	12.5(1)	11.8(2)	13.9(1)
$[M(\mathbf{L^1})]^{2+} + H^+ \rightleftharpoons [M(H\mathbf{L^1})]^{3+}$			2.5(2)	3.2(1)	
$M^{2+} + \mathbf{L^2} \rightleftharpoons [M(\mathbf{L^2})]^{2+}$	16.82(4)	14.85(5)	10.4(1)	11.1(1)	
$[M(\mathbf{L^2})]^{2+} + H^+ \rightleftharpoons [M(H\mathbf{L^2})]^{3+}$		2.8(1)			
$M^{2+} + \mathbf{L^3} \rightleftharpoons [M(\mathbf{L^3})]^{2+}$	> 17	13.8(1)	10.87(7)	12.35(8)	13.2(1)

[a] $MeCN/H_2O$ (1:1 v/v), 0.10 M NMe_4Cl, 298.1 K. [b] Potentiometric study in $MeCN/H_2O$ (1:1 v/v) was limited to the acidic pH region because of complex precipitation at neutral pH values. [c] The low solubility of the complex does not allow the determination of the stability constant of the 1:1 Hg^{II} complex with $\mathbf{L^2}$.

the CFSE (Crystal Field Stabilization Energy) of its complexes.

Polyamine ligands are also known for the similarities in their binding abilities toward Zn^{II}, Cd^{II}, and Pb^{II}. Recently, it has been proposed that the stability of the Zn^{II}, Cd^{II}, and Pb^{II} complexes with amine ligands bearing heteroaromatic side arms, such as quinoline or pyridine, could be influenced by steric crowding of ligands around the metal cation.[56]

In particular, the largest metal cations Pb^{II} and, to a lesser extent, Cd^{II}, can better accommodate sterically crowded ligands, giving rise to stronger coordination bonds and affording more stable complexes than the smaller Zn^{II}. In the present case, steric crowding of ligands increases in the order $\mathbf{L^2} < \mathbf{L^3} < \mathbf{L^1}$. At a first glance, data in Table 4 seem to contradict the hypothesis of steric control of complex stability. In fact, the smaller Zn^{II} ion forms more stable complexes than Cd^{II} and Pb^{II} with all three ligands and, in the case of the most sterically hindered ligand $\mathbf{L^1}$, the stability increases as the dimension of the metal cations decreases, that is, in the order $Pb^{II} < Cd^{II} < Zn^{II}$. This order is opposite to that expected if the complex stability is mainly determined by steric crowding of ligands. On the other hand, a more accurate inspection of data in Table 4 also shows that the smaller Zn^{II} forms a more stable complex with the less sterically hindered ligand $\mathbf{L^2}$, while the larger Cd^{II} and Pb^{II} give less stable complexes with this ligand, indicating that steric hindrance of ligands may also play a role in determining the stability of the present complexes. However, these observations suggest that the stability of Zn^{II}, Cd^{II}, and Pb^{II} complexes with $\mathbf{L^1}-\mathbf{L^3}$ depends on factors other than steric crowding. For example, all three ligands feature hydrophobic quinoline side-arms and, therefore, a marked desolvation of the metal cations upon complex formation is expected. From this point of view, the higher stability observed for the Zn^{II} complexes with all three ligands could be ascribed to the fact that this metal cation is more solvated than the larger Cd^{II} and Pb^{II} cations and thus it undergoes a greater degree of desolvation upon complexation, with a consequent gain in translational entropy. Clearly, the fact that Zn^{II} forms the most stable complex with the less hydrophobic ligand $\mathbf{L^2}$ cannot be explained in terms of desolvation only, but can be reasonably ascribed also to the less hindered structure of this ligand, which can better adapt itself to the stereochemical requests of this small metal cation, giving rise to stronger Zn−N coordination bonds. This hypothesis seems to be confirmed by the Zn−N bond distances observed in the crystal structure of the Zn^{II} complex with $\mathbf{L^2}$, which are somewhat shorter than those found in the structures of the complexes with $\mathbf{L^1}$ and $\mathbf{L^3}$ (see below).

Metal Complexation: Solid State. From the complexation reaction of $\mathbf{L^1}-\mathbf{L^3}$ with the appropriate metal salts in MeCN, 1:1 metal complexes with Cu^{II}, Zn^{II}, Cd^{II}, Hg^{II}, and Pb^{II} were isolated in the solid state (see Supporting Information); crystals suitable for X-ray structural analysis were obtained for the complexes $[Cu(\mathbf{L^1})](BF_4)_2$ (**1**), $[Zn(\mathbf{L^1})](BF_4)_2$ (**2**), $[Cd(\mathbf{L^1})](ClO_4)_2$ (**3**), $[Hg(\mathbf{L^1})](NO_3)_2$ (**4**), $[Pb(\mathbf{L^1})](ClO_4)_2 \cdot MeCN$ (**5**), $[Zn_2Cl_2(\mathbf{L^2})_2](BF_4)_2 \cdot {}^1/_2 MeNO_2 \cdot H_2O$ (**6**), $[Cu(\mathbf{L^3})](ClO_4)_2$ (**7**), $[Zn(\mathbf{L^3})(NO_3)]NO_3$ (**8**), $[Cd(\mathbf{L^3})(NO_3)_{0.82}Cl_{0.18}]NO_3$ (**9**), and $[Hg(\mathbf{L^3})](ClO_4)_2 \cdot MeCN$ (**10**). In **1**−**5**, $\mathbf{L^1}$ acts as a hexadentate ligand and the metal(II) ions are in a *pseudo*-octahedral (Cu^{II} and Zn^{II} in **1** and **2**, respectively), *pseudo*-trigonal prismatic (Cd^{II} and Hg^{II} in **3** and **4**, respectively) or highly trigonal distorted *pseudo*-octahedral (Pb^{II} in **5**) environments, each defined by six nitrogen atoms, that is, three tertiary amine nitrogen donors from the [9]aneN_3 backbone, and three quinoline nitrogen donors (Figure 2, Supporting Information, Figure S6, Table 5). The ranges for the $M-N_{(tertiary\ amine)}$ and $M-N_{(quinoline)}$ distances are respectively 2.208(3)−2.028(3) and 2.527(4)−2.072(3) Å in **1**, 2.2327(15)−2.1439(15) and 2.2336(14)−2.2070(15) Å in **2**, 2.393(5)−2.367(6) and 2.395(5)−2.350(6) Å in **3**, 2.456(5)−2.402(6) and 2.473(5)−2.340(5) Å in **4**, and 2.536(4)−2.505(4) and 2.833(6)−2.712(4) Å in **5**. On increasing the ionic radius, the metal center is displaced further from the [9]aneN_3 ring cavity in the direction of the quinoline manifold. In **1**, one of the $Cu-N_{(quinoline)}$ distances, Cu(1)−N(5), is significantly longer than the other two, and also longer than the mean length for Cu−N bonds to quinoline and quinoline-like ligands (1,10-phenanthroline, 8-hydroxyquinoline, etc.) found in the CSD: 2.05(7) Å (1376 hits).[57] A similar degree of distortion is not observed in the 1:1 copper(II) complex of the structural analogue of $\mathbf{L^1}$ having pyridyl pendant arms where the $Cu-N_{(pyridine)}$ bonds range from 1.995(8) to 2.211(9) Å.[58] The $Zn-N_{(quinoline)}$ bonds in **2** also appears to be slightly longer than normal; however, all three are within the range of variability found in the literature: the mean length for Zn−N bonds to quinoline and quinoline-like ligands found in the CSD is 2.14(6) Å (468 hits).[57] Interestingly, the average $Zn-N_{(pyridine)}$

(56) Williams, N. J.; Gan, W.; Reibenspies, J. H.; Hancock, R. D. *Inorg. Chem.* **2009**, *48*, 1407.

(57) Data were retrieved from CSD using CCDC software (2009, v.5.30).

(58) Han, W.; Wang, Z.-W.; Xie, C.-Z.; Liu, Z.-Q.; Yan, S.-P.; Liao, D.-Z.; Jaing, Z.-H.; Cheng, P. *J. Chem. Crystallogr.* **2004**, *34*, 495.

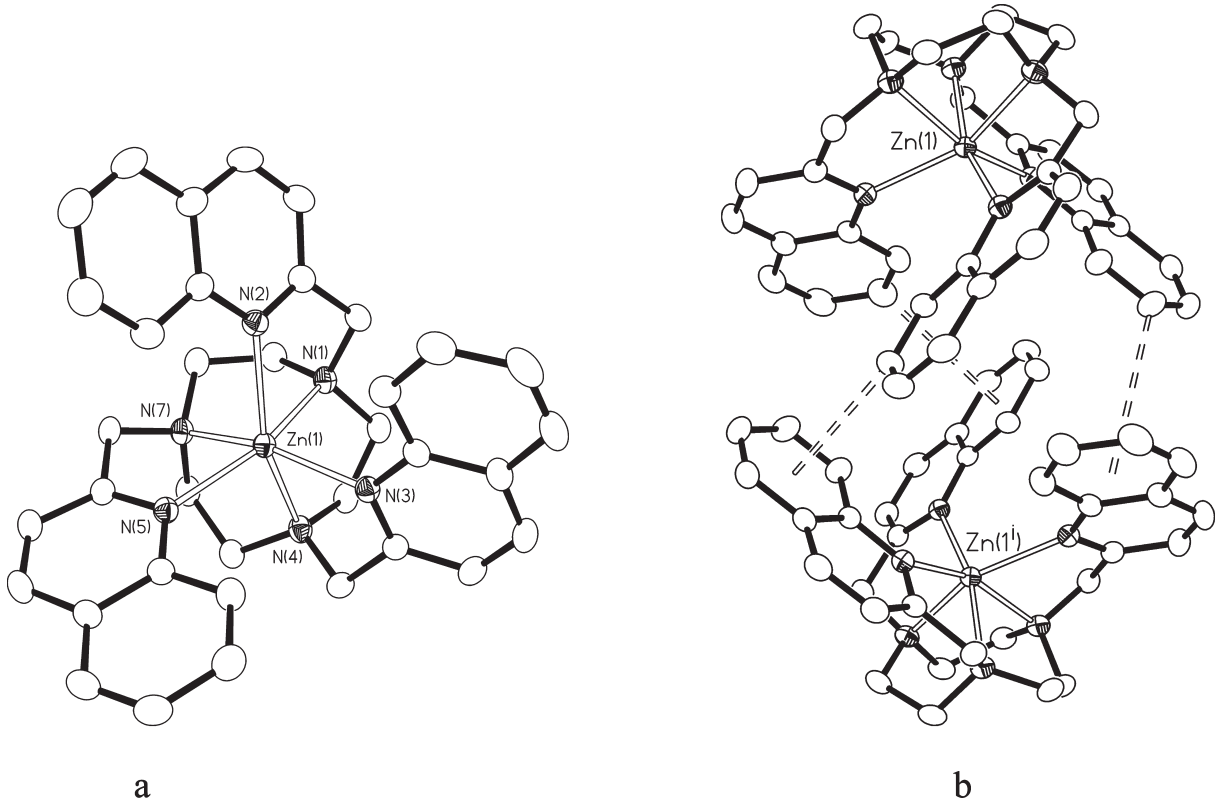

Figure 2. (a) View of the complex cation $[Zn(\mathbf{L^1})]^{2+}$ in **2** in its enantiomeric form $\Delta(\lambda\lambda\lambda)_5(\delta\delta\delta)_5$ (see text) with the numbering scheme adopted. Displacement ellipsoids are drawn at the 50% probability level. Hydrogen atoms and counteranions have been omitted for clarity. (b) Pairs of Δ and Λ enantiomers of $[Zn(\mathbf{L^1})]^{2+}$ in the crystal packing of **2** interacting via edge-to-face π-stacking interactions (mean distance C···centroid of the aromatic ring 3.6 Å; $i = -x, 1-y, -z$).

Table 5. Selected Bond Distances (Å) and Angles (deg) for $[Cu(\mathbf{L^1})](BF_4)_2$ (**1**), $[Zn(\mathbf{L^1})](BF_4)_2$ (**2**), $[Cd(\mathbf{L^1})](ClO_4)_2$ (**3**), $[Hg(\mathbf{L^1})](NO_3)_2$ (**4**), $[Pb(\mathbf{L^1})](ClO_4)_2 \cdot MeCN$ (**5**), and $[Zn_2Cl_2(\mathbf{L^2})_2](BF_4)_2 \cdot {}^1/_2MeNO_2 \cdot H_2O$ (**6**)[a]

	1	**2**	**3**	**4**	**5**	**6**
M(1)−N(1)	2.028(3)	2.2327(15)	2.367(6)	2.450(5)	2.505(4)	2.189(5)
M(1)−N(2)	2.170(3)	2.2701(15)	2.371(5)	2.340(5)	2.799(5)	2.180(4)
M(1)−N(3)/X(1)	2.072(3)	2.1897(14)	2.395(5)	2.473(5)	2.712(4)	2.3665(16)
M(1)−N(4)	2.208(3)	2.2070(15)	2.393(5)	2.402(6)	2.508(4)	2.150(5)
M(1)−N(5)/X(1^{i})	2.527(4)	2.2336(14)	2.350(6)	2.378(6)	2.833(6)	2.6908(15)
M(1)−N(7)	2.196(3)	2.1439(15)	2.389(6)	2.456(5)	2.536(4)	2.126(5)
N(1)−M(1)−N(2)	81.3(1)	76.20(5)	72.6(2)	72.0(2)	63.9(1)	76.63(17)
N(1)−M(1)−N(3)/X(1)	164.7(1)	95.02(5)	108.2(2)	108.9(2)	85.8(1)	176.37(12)
N(1)−M(1)−N(4)	84.3(1)	78.50(5)	74.4(2)	74.0(2)	71.7(2)	79.97(19)
N(1)−M(1)−N(5)/X(1^{i})	91.4(1)	158.64(5)	144.9(2)	140.9(2)	132.3(1)	94.93(14)
N(1)−M(1)−N(7)	82.5(1)	80.68(5)	75.3(2)	73.4(2)	70.5(1)	81.69(19)
N(2)−M(1)−N(3)/X(1)	103.4(1)	102.53(5)	104.5(2)	103.1(2)	118.8(1)	106.91(13)
N(2)−M(1)−N(4)	102.7(1)	154.69(6)	143.2(2)	140.7(2)	134.6(1)	153.52(19)
N(2)−M(1)−N(5)/X(1^{i})	103.7(1)	105.96(5)	106.0(2)	109.0(2)	120.0(1)	82.98(12)
N(2)−M(1)−N(7)	163.2(1)	94.49(5)	111.6(2)	113.0(2)	86.0(2)	105.86(19)
N(3)/X(1)−M(1)−N(4)	80.5(1)	78.93(5)	71.2(2)	70.2(2)	64.7(1)	96.40(15)
N(3)/X(1)−M(1)−N(5)/X(1^{i})	101.4(1)	105.00(5)	106.0(2)	108.7(2)	119.6(1)	84.85(5)
N(3)/X(1)−M(1)−N(7)	93.5(1)	160.95(6)	142.8(2)	142.0(2)	133.9(1)	97.88(14)
N(4)−M(1)−N(5)/X(1^{i})	152.2(1)	97.85(5)	110.3(2)	109.7(2)	83.5(1)	86.86(14)
N(4)−M(1)−N(7)	79.8(1)	82.02(6)	74.5(2)	74.5(2)	70.4(2)	82.6(2)
N(5)/X(1^{i})−M(1)−N(7)	72.4(1)	77.97(5)	72.9(2)	70.7(2)	62.9(2)	169.37(15)
M(1)−Cl(1)−M(1^{i})						95.15(5)

[a] X(1) = Cl(1), X(1^{i}) = Cl(1^{i}) in **6**; $i = 1-x, -y, 1-z$.

bond length in the zinc(II) complex of the structural analogue of $\mathbf{L^1}$ having pyridyl pendant arms is 2.139 Å.[58] The very small possible distortion of the $Zn-N_{(aromatic)}$ bonds in $[Zn(\mathbf{L^1})]^{2+}$ as compared to the 1:1 complex between Zn^{II} and the [9]aneN$_3$ derivative featuring pyridyl pendant arms could be attributed to an increased steric crowding determined by the bulkier quinolyl groups.[56] In this respect, no sign of a $Zn-N_{(quinoline)}$ bond-length distortion due to steric crowding effects appears to be present in $[Zn(\mathbf{TQA})\text{-}H_2O]^{2+}$ [mean $Zn-N_{(quinoline)}$ = 2.132 Å, Scheme 1].[56] On the contrary, the presence of a fourth bulky quinolyl

group in **TQEN** (Scheme 1) causes two of the four $Zn-N_{(quinoline)}$ bonds in $[Zn(\mathbf{TQEN})]^{2+}$ to be very long at 2.3711(15) and 2.4007(15) Å, while the remaining two are well within the range for normal $Zn-N_{(quinoline)}$ bonds 2.1543(14) and 2.1271(14) Å.[56,59] The $M-N_{(quinoline)}$ bond distances in $[Cd(\mathbf{L^1})]^{2+}$ and $[Hg(\mathbf{L^1})]^{2+}$ exhibit no sign of steric crowding effects [the mean length for M−N bonds to quinoline and quinoline-like ligands found in the CSD is 2.36(5) Å for Cd^{II} (282 hits) and 2.44(13) Å for Hg^{II} (39 hits)].[57] Also the $Pb-N_{(quinoline)}$ distances observed in $[Pb(\mathbf{L^1})]^{2+}$ appear to be slightly longer than normal, close to the upper edge of the range of variability found in the literature: the mean length for Pb−N bonds to quinoline and quinoline-like ligands found in the CSD is 2.60(10) (128 hits).[57] This could also be determined by the fact they are closer than the opposite $Pb-N_{(tertiary\ amine)}$ bonds to the probable site of the sterically active 6*s* lone pair.

The $[M(\mathbf{L^1})]^{2+}$ complex cations in **1**−**5** are chiral; they adopt both Δ and Λ configurations resembling a right-handed and left-handed three-bladed screw propeller, respectively.[60] The three five-membered chelate rings of the coordinated [9]aneN$_3$ framework as well as the three five membered chelate rings of the quinolyl-functionalized pendant arms adopt a $(\delta\delta\delta)_5$ or a $(\lambda\lambda\lambda)_5$ conformation. Thus, for the complex cations $[M(\mathbf{L^1})]^{2+}$ (M = Cu^{II}, Zn^{II}, Pb^{II}) the two enantiomeric forms $\Delta(\lambda\lambda\lambda)_5(\delta\delta\delta)_5$ and $\Lambda(\delta\delta\delta)_5(\lambda\lambda\lambda)_5$ are present in equal amounts in the unit cells of **1**, **2**, and **5**; whereas, $[Cd(\mathbf{L^1})]^{2+}$ and $[Hg(\mathbf{L^1})]^{2+}$, in **3** and **4**, respectively, similarly adopt the enantiomeric forms $\Delta(\delta\delta\delta)_5(\delta\delta\delta)_5$ and $\Lambda(\lambda\lambda\lambda)_5(\lambda\lambda\lambda)_5$ [the first bracket refers to conformations adopted by the three chelate rings of the [9]aneN$_3$ backbone]. The two enantiomeric forms of the complex cations $[M(\mathbf{L^1})]^{2+}$ in **1**−**5** interact via edge-to-face or face-to-face π-stacking interactions at the quinolyl groups. In particular, in the case of $[Cu(\mathbf{L^1})]^{2+}$ and $[Zn(\mathbf{L^1})]^{2+}$ in **1** and **2**, respectively, these interactions involve all three quinolyl groups of each enantiomer, and pairs of interacting Λ and Δ enantiomers, related by an inversion center, define a hydrophobic cavity of approximate radius of 4 Å (Figure 2b for Zn^{II}). In the cases of **3**, **4**, and **5**, only two quinolyl groups of each enantiomer are involved in π-stacking interactions, and isolated dimers (**3**) or chains of alternating interacting Λ and Δ enantiomers (**4**, **5**) can be envisaged in the crystal lattice (Supporting Information, Figures S7−S9).

From the complexation reaction of $\mathbf{L^2}$ with the appropriate metal salts (see Experimental Section and Supporting Information), we were able to grow single crystals only of the complex $[Zn_2(\mathbf{L^2})_2(Cl)_2](BF_4)_2\cdot{}^1/_2MeNO_2\cdot H_2O$ (**6**). The crystal structure confirmed the formation of the dichloro-bridged binuclear complex $[Zn_2Cl_2(\mathbf{L^2})_2]^{2+}$ lying across a crystallographic inversion center (Figure 3, Table 5). Each Zn^{II} in this complex cation is six-coordinate with the four N-donors of $\mathbf{L^2}$ and the two bridging Cl^- ligands defining a distorted octahedral environment. The $Zn-N_{(tertiary\ amine)}$ bond distances range between 2.126(5) and 2.189(5) Å, whereas the $Zn-N_{(quinoline)}$ bond length is 2.180(4) Å. Pairs of complex cations $[Zn_2Cl_2(\mathbf{L^2})_2]^{2+}$ interact via face-to-face π-stacking interactions at the quinolyl

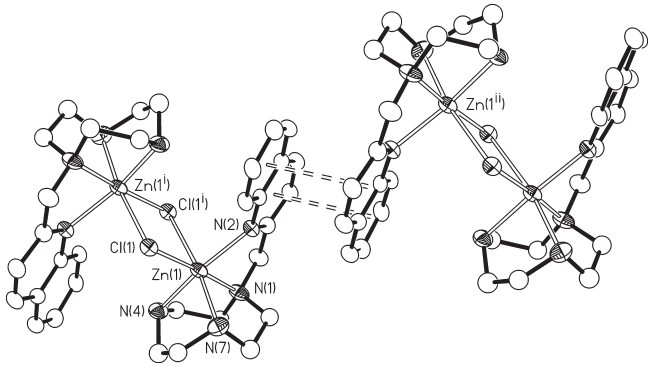

Figure 3. View of the complex cation $[Zn_2Cl_2(\mathbf{L^2})]^{2+}$ in **6** with the numbering scheme adopted. Displacement ellipsoids are drawn at the 40% probability level. Hydrogen atoms and counteranions have been omitted for clarity (i = 1 − *x*, −*y*, 1 − *z*; ii = 1 − *x*, 1 − *y*, 1 − *z*).

group (interplanar distance between aromatic rings 3.5 Å) to give extended chains along the *b* axis (Figure 3).

In comparison to that of [9]aneN$_3$,[29] the coordination chemistry of [9]aneN$_2$S is less explored; much fewer functionalized pendant arm derivatives of this mixed thia-aza small ring crown have been synthesized and studied.[30,31] From the complexation reaction of $\mathbf{L^3}$ with the appropriate metal salts (see Experimental Section and Supporting Information), we were able to grow single crystals of the complexes $[Cu(\mathbf{L^3})](ClO_4)_2$ (**7**), $[Zn(\mathbf{L^3})(NO_3)]NO_3$ (**8**), $[Cd(\mathbf{L^3})(NO_3)_{0.82}Cl_{0.18}]NO_3$ (**9**), and $[Hg(\mathbf{L^3})](ClO_4)_2\cdot MeCN$ (**10**). The crystal structures confirmed the formation of 1:1 metal-to-ligand complex species in all cases (Figure 4, Table 6). The metal center in $[Cu(\mathbf{L^3})]^{2+}$ is five coordinated by the pentadentate $\mathbf{L^3}$ within a coordination environment that is intermediate between square-based pyramidal and trigonal bipyramidal. The irregular coordination geometry of $[Cu(\mathbf{L^3})]^{2+}$ in the solid state, presumably determined by the steric repulsion between the bulky quinolyl groups, is estimated to be about 40% along the pathway of distortion from square pyramidal toward trigonal bipyramidal, according to the criterion of Addison and Rao.[61] The Cu−N and Cu−S bond distances (Table 6) are, however, very close to those observed in the 1:1 copper(II) complex of the structural analogue of $\mathbf{L^3}$ having pyridyl pendant arms where the smaller pyridyl groups allow a more regular square-based pyramidal coordination geometry at the metal center (the four N-donors lie on a plane, with the metal center displaced 0.22 Å out of this plane toward the apical S-donor, and the Cu−S vector is almost perpendicular to the basal coordination plane).[30]

The addition of $Zn(NO_3)_2$ to $\mathbf{L^3}$ afforded the compound **8**, the structure of which revealed a distorted octahedral geometry for Zn^{II}, with the macrocycle facially capping the metal center (Figure 4b, Table 6). The coordination sphere in the complex $[Zn(\mathbf{L^3})NO_3]^+$ is completed by the two quinolyl donors and a monodentate nitrate ligand. The equatorial plane is defined by the two macrocyclic N-donors, one of the two pendant arm quinolyl N-donors and the nitrate oxygen. The axial sites are occupied by the S-donor of the macrocycle and the remaining quinolyl N-donor [N(1)−Zn(1)−S(1) 162.46(15) [161.97(15)°], N(1)−Zn(1)−N(7) 95.4(2)

(59) Mikata, Y.; Wakamatsu, M.; Yano, S. *Dalton Trans.* **2005**, 545.
(60) Weighardt, K.; Schöffmann, E.; Nuber, B.; Weiss, J. *Inorg. Chem.* **1986**, *25*, 4877.
(61) Addison, A. W.; Rao, N. *J. Chem. Soc., Dalton Trans.* **1984**, 1349.

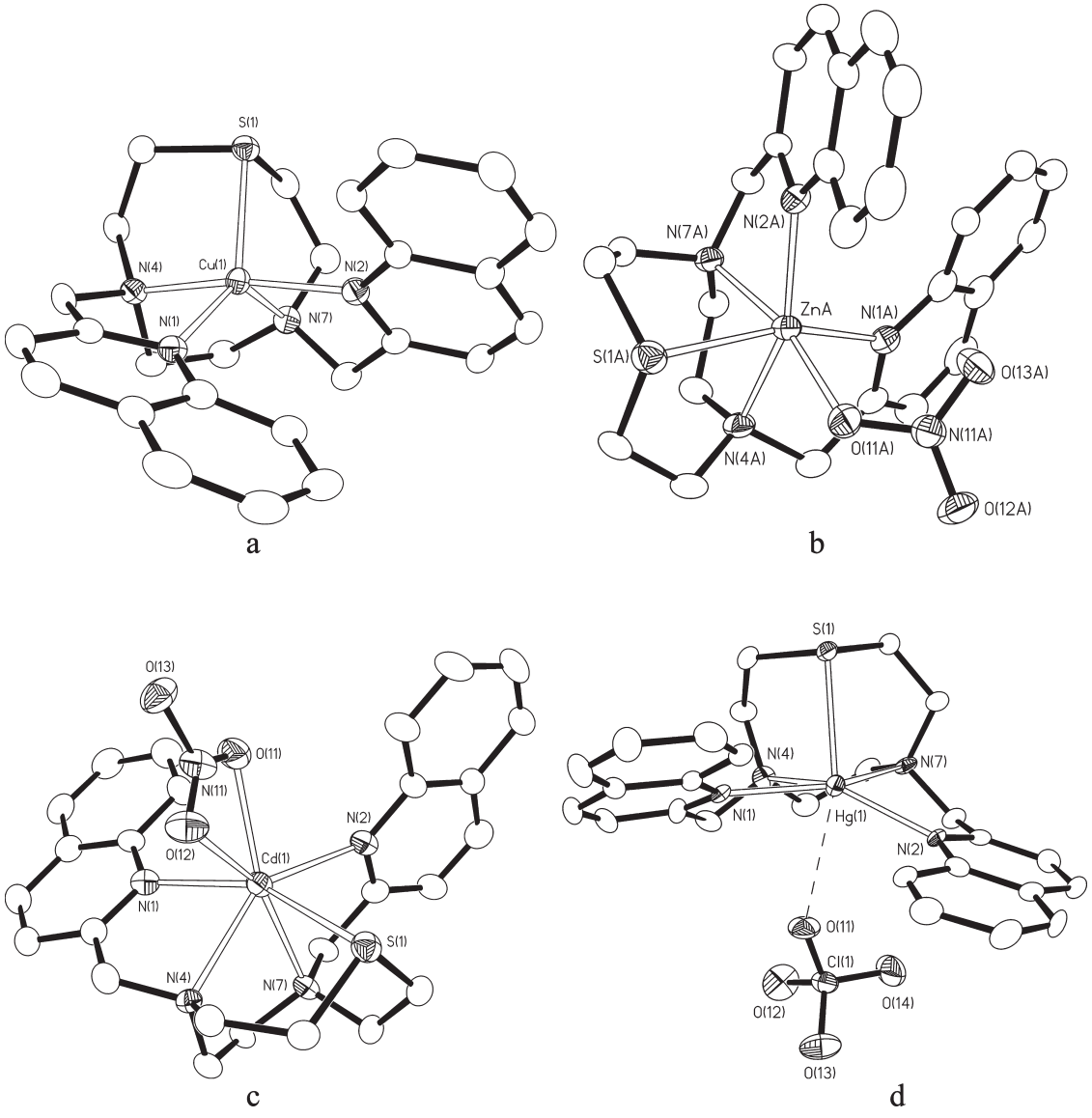

Figure 4. View of the complex cations $[Cu(\mathbf{L}^3)]^{2+}$ in **7** (a), $[Zn(\mathbf{L}^3)(NO_3)]^{+}$ in **8** (b), $[CdNO_3(\mathbf{L}^3)]^{+}$ in **9** (c), and $[Hg(\mathbf{L}^3)]^{2+}$ in **10** (d) with the numbering schemes adopted. Displacement ellipsoids are drawn at the 50% probability level. Hydrogen atoms, counteranions, and solvent molecules have been omitted for clarity.

[95.1(2)], Table 6, Figure 4b]. Therefore, in contrast to $[Cu(\mathbf{L}^3)]^{2+}$, in $[Zn(\mathbf{L}^3)NO_3]^{+}$, the presence of an exogenous nitrate ligand imposes an expansion of the coordination number from five to six, and a rearrangement of the coordination geometry at the metal center. This allows closer approach between one of the quinolyl N-donors and the S-donor of the pentadentate ligand $\mathbf{L}^3$ within a distorted octahedral geometry, thus reducing the steric repulsion between the two quinolyl groups. A similar disposition of the donor groups has been observed in the 1:1 nickel(II) complex of the structural analogue of $\mathbf{L}^3$ having pyridyl pendant arms.[30]

In **9** (Figure 4c, Table 6), overall N_4SO_2 seven-coordination is apparently achieved at the metal center via the five donor atoms of $\mathbf{L}^3$ and two O-donors derived from one terminal asymmetrical bidentate NO_3^- ligand or from a chloride ligand (Table 6). The coordination environment at Cd^{II} is very similar to that observed for Zn^{II} in $[Zn(\mathbf{L}^3)NO_3]^{+}$ (Figure 4, panels b and c) and could also be described as *pseudo*-octahedral if the asymmetrical bidentate nitrate ligand is considered to formally occupy one coordination site of a distorted octahedron.

Interestingly, also in $[Hg(\mathbf{L}^3)]^{2+}$ (Figure 4d, Table 6) the pentadentate ligand imposes on the metal center an irregular five coordination geometry similarly to that observed in $[Cu(\mathbf{L}^3)]^{2+}$. In this case, the index of trigonality is only 15%,[61] and the metal center interacts only very weakly with the oxygen atom of a ClO_4^- anion located in the hemisphere left free by $\mathbf{L}^3$ [Hg(1)−O(11) 2.829(5)Å, [S(1)−Hg(1)−O(11) 162.98(15)°]. As observed in the species $[M(\mathbf{L}^1)]^{2+}$ ($M = Zn^{II}$, Cd^{II}, Hg^{II}, Pb^{II}), also in the structurally characterized complexes with $\mathbf{L}^3$, the bond distances between the metal center and the donor atoms of the ligand, increase on increasing the ionic radius of the metal ion. The $M-N_{(quinoline)}$ bond distances observed in $[Zn(\mathbf{L}^3)NO_3]^{2+}$ and $[Cd(\mathbf{L}^3)NO_3]^{+}$ are very close to normal, whereas the $Hg-N_{(quinoline)}$ ones appear rather shorter than the average value, but well within the range of variability found in the literature (see above). Also, in **7**−**10** edge-to-face and face-to-face π-stacking interactions are observed between the

Table 6. Selected Bond Distances (Å) and Angles (deg) for $[Cu(\mathbf{L^3})](ClO_4)_2$ (**7**), $[Zn(\mathbf{L^3})(NO_3)]NO_3$ (**8**),[a] $[Cd(\mathbf{L^3})(NO_3)_{0.82}Cl_{0.18}]NO_3$ (**9**), and $[Hg(\mathbf{L^3})](ClO_4)_2 \cdot MeCN$ (**10**)[b]

	7	8[c]	9[d]	10
M(1)−N(1)	2.078(2)	2.173(5) [2.165(5)]	2.320(4)	2.275(6)
M(1)−N(2)	1.981(2)	2.149(5) [2.152(5)]	2.476(3)	2.214(5)
M(1)−N(4)	2.013(2)	2.208(5) [2.202(5)]	2.432(3)	2.494(6)
M(1)−N(7)	2.112(2)	2.200(5) [2.208(5)]	2.401(3)	2.493(6)
M(1)−S(1)	2.4402(8)	2.5218(18) [2.5419(18)]	2.6944(12)	2.6412(17)
M(1)−X		2.100(5) [2.099(5)]	2.323(4) [2.508(4)]	
N(1)−M(1)−N(2)	101.21(9)	105.6(2) [107.1(2)]	116.54(12)	137.1(2)
N(1)−M(1)−N(4)	82.52(9)	80.0(2) [79.6(2)]	73.76(12)	72.5(2)
N(1)−M(1)−N(7)	129.98(10)	95.4(2) [95.1(2)]	95.99(11)	143.7(2)
N(1)−M(1)−S(1)	139.85(7)	162.46(15) [161.97(15)]	151.78(10)	92.46(14)
N(1)−M(1)−X		89.9(2) [92.4(2)]	84.78(13) [86.33(13)]	
N(2)−M(1)−N(4)	165.86(10)	156.0(2) [155.8(2)]	143.89(11)	134.5(2)
N(2)−M(1)−N(7)	81.80(10)	77.5(2) [77.2(2)]	71.21(11)	74.6(2)
N(2)−M(1)−S(1)	98.45(7)	91.81(15) [90.47(15)]	88.45(9)	121.47(14)
N(2)−M(1)−X		112.8(2) [112.4(2)]	87.90(13) [133.87(13)]	
N(4)−M(1)−N(7)	85.39(10)	78.74(19) [79.1(2)]	73.35(11)	71.4(2)
N(4)−M(1)−S(1)	86.82(7)	83.29(15) [82.72(16)]	78.24(8)	79.33(15)
N(4)−M(1)-X		90.26(19) [90.1(2)]	128.18(12) [78.66(13)]	
N(7)−M(1)−S(1)	87.19(7)	86.37(14) [84.87(14)]	79.12(9)	77.61(13)
N(7)−M(1)−X		166.73(19) [165.49(19)]	157.09(14) [149.97(13)]	
S(1)−M(1)−X		84.98(14) [84.18(14)]	110.46(11) [84.79(10)]	
O(11)−Cd(1)−O(12)			52.91(14)	

[a] Two independent molecules of $[Zn(\mathbf{L^3})(NO_3)]^+$ are present in the asymmetric unit of **8**. [b] X = monodentate $N(11)O_3$ (**8**), bidentate $N(11)O_3$ (**9**) (see Figure 4). [c] Bond distances and angles observed in both independent units are reported. [d] Where two values are reported, the first refers to bond distances and angles involving O(11) and the second to bond distances and angles involving O(12) (see Figure 4c).

quinolyl groups of the complex cations (see Supporting Information, Figure S10 for $[Cu(\mathbf{L^3})]^{2+}$).

Optical Response of $\mathbf{L^1}$−$\mathbf{L^3}$ to the Presence of Cu^{II}, Zn^{II}, Cd^{II}, Hg^{II}, and Pb^{II}. Many "OFF-ON" ligands for sensing Zn^{II} are quinoline-based molecules which take advantage of a photoinduced electron-transfer (PET) mechanism of fluorescence.[6,15,38,56,59,62−66] These probes also exhibit a chelation enhancement of fluorescence (CHEF effect) in the presence of Cd^{II}. Very recently, the idea has emerged that the relative strength of the CHEF effect for the small Zn^{II} as compared to larger Cd^{II} ion might be determined by steric crowding in the corresponding complexes: a Zn−N bond length elongation by steric crowding would partially restore the PET quenching mechanism and hence cause a lower CHEF effect for Zn^{II} relative to Cd^{II}.[56] Therefore, we decided to investigate the optical response of $\mathbf{L^1}$−$\mathbf{L^3}$ to the presence of Cu^{II}, Zn^{II}, Cd^{II}, Hg^{II}, and Pb^{II} in the solvent mixture $MeCN/H_2O$ (1:1 v/v) and in H_2O. The absorption spectra of $MeCN/H_2O$ (1:1 v/v, 25 °C) solutions of $\mathbf{L^1}$−$\mathbf{L^3}$ present a large unstructured band at around 230 nm and three other less intense bands at around 275, 300, and 315 nm (see the Experimental Section). In the same mixture of solvents all three ligands exhibit an emission band at 380 nm with very low fluorescence quantum yield ($\Phi = 0.0007$), when excited at 316 nm.[67] This very low yield can be attributed to a PET process between the tertiary nitrogen atoms of the macrocyclic moieties and the quinoline fragment(s).

Significant and parallel changes were observed in the UV−vis spectra of $\mathbf{L^1}$−$\mathbf{L^3}$ in $MeCN/H_2O$ (1:1 v/v, 25 °C) buffered at pH = 7.4 (MOPS) upon addition of each metal ion investigated (Figure 5a for $\mathbf{L^1}$, Supporting Information, Figures S11a and S12a for $\mathbf{L^2}$ and $\mathbf{L^3}$, respectively, in the case of Zn^{II}). In particular, the band at around 230 nm either decreases or increases in intensity, and generally shifts to slightly higher wavelengths. Furthermore, the band at around 275 nm decreases and those at around 300 and 315 nm very slightly increase in intensity; the presence in all cases of well-defined isosbestic point(s) suggests the presence of only two species in equilibrium. Because the fluorescence of quinoline-based molecular sensors is often pH sensitive, we initially studied the effect of pH on the fluorescence of both $\mathbf{L^1}$, $\mathbf{L^2}$, or $\mathbf{L^3}$ and of their 1:1 metal complexes with Cu^{II}, Zn^{II}, Cd^{II}, Hg^{II}, or Pb^{II} in $MeCN/H_2O$ (1:1 v/v, 25 °C). For none of the three ligands does the fluorescence "OFF" state change significantly over the range of pH investigated (Figure 5b for $\mathbf{L^1}$, Supporting Information, Figures S11b and S12b for $\mathbf{L^2}$ and $\mathbf{L^3}$, respectively). A significant CHEF effect is only observed in the presence of Zn^{II} (1 equiv) in the pH range 3.0−10.0, with the maximum effect around pH 7.0. The presence of the other metal ions does not seem to significantly affect the OFF state of the sensors (Figures 5b, Supporting Information, Figures S11b and S12b). The subsequent return of the ligands to an OFF state at higher pH values (>9.0−10.0) could be the result of the formation of hydroxylated species. We

(62) Mikata, Y.; Wakamatsu, M.; Kawamura, A.; Yamanaka, N.; Yano, S.; Odani, A.; Morihiro, K.; Tamotsu, S. *Inorg. Chem.* **2006**, *45*, 9262.
(63) Wu, D.-Y.; Xie, L.-X.; Zhang, C.-L.; Duan, C.-Y.; Zhao, Y.-G.; Guo, Z.-J. *Dalton Trans.* **2006**, 3528.
(64) Mikata, Y.; Yamanata, A.; Yamashita, A.; Yano, S. *Inorg. Chem.* **2008**, *47*, 7295.
(65) Gan, W.; Jones, S. B.; Reibenspies, J. H.; Hancock, R. D. *Inorg. Chim. Acta* **2005**, *358*, 3958.
(66) Kimber, M. C.; Mahadevan, I. B.; Lincoln, S. F.; Ward, A. D.; Tiekink, E. R. T. *J. Org. Chem.* **2000**, *65*, 8204.
(67) The excitation wavelength for $\mathbf{L^1}$−$\mathbf{L^3}$, as for other quinoline-based fluorescent chemosensors reported in the literature, is taken at the maximum of the lowest energy absorption band whose absorbance very slightly changes on adding metal ions (see refs 38, 56, 59, 62−66). We have verified that when exciting at the isosbestic wavelengths, the fluorescence intensity emission observed in the presence of metal ions is much lower or approaches zero depending on the closeness of the isosbestic point to the lowest energy absorption band of the ligands. However, for all the spectrofluorimetric titrations described in the paper, emission data were corrected for the absorbed light when necessary (see Experimental Section).

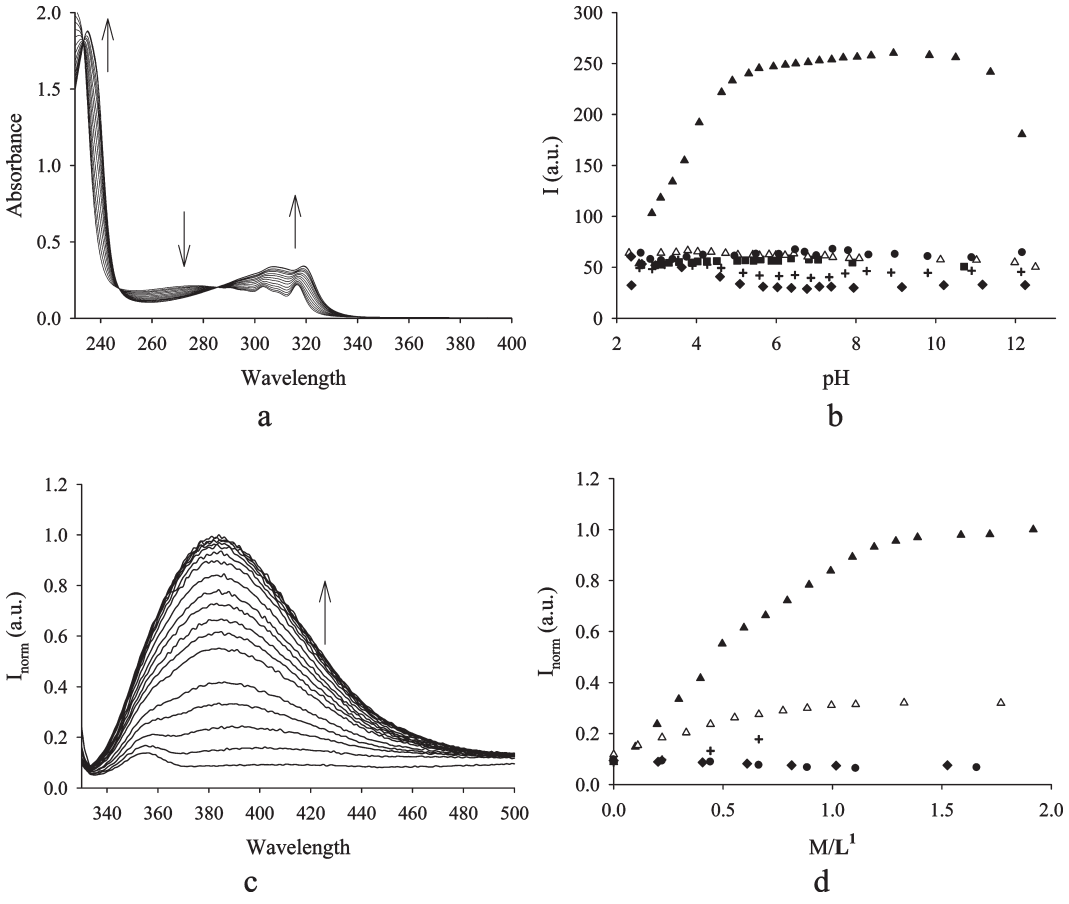

Figure 5. (a) Changes in the absorption spectrum of $\mathbf{L^1}$ in MeCN/H_2O [1:1 v/v, pH = 7.4 (MOPS), 25 °C] upon addition of increasing amounts of Zn^{II}, isosbestic points occur at 285, 248, and 234 nm. (b) Effect of pH on the fluorescence intensity at 380 nm of $\mathbf{L^1}$ [2.5×10^{-5} M, MeCN/H_2O (1:1 v/v), 25 °C] in the absence (■) and presence of 1 equiv of Cu^{II} (●), Zn^{II} (▲), Cd^{II} (Δ), Hg^{II} (♦), and Pb^{II} (+). (c) Changes in the emission spectrum of $\mathbf{L^1}$ [2.5×10^{-5} M, MeCN/H_2O (1:1 v/v), pH = 7.4 (MOPS), 25 °C] upon addition of increasing amounts of Zn^{II}. (d) Normalized fluorescence intensity/molar ratio plots for $\mathbf{L^1}$ [2.5×10^{-5} M, MeCN/H_2O (1:1 v/v), pH = 7.4 (MOPS), 25 °C] in the presence of increasing amounts of Cu^{II} (●), Zn^{II} (▲), Cd^{II} (△) and Hg^{II} (♦), the addition of a Pb^{II} (+) amount higher than 0.6 equiv appeared to cause precipitation (in all experiments λ_{ex} = 316 nm, λ_{em} = 380 nm).

therefore performed spectrofluorimetric titrations of $\mathbf{L^1}$, $\mathbf{L^2}$, or $\mathbf{L^3}$ with Cu^{II}, Zn^{II}, Cd^{II}, Hg^{II}, or Pb^{II} in MeCN/H_2O (1:1 v/v, 25 °C) solutions buffered at pH 7.4 with MOPS. Indeed, a significant CHEF effect was observed upon addition of Zn^{II} up to a Zn/**L** (L = $\mathbf{L^1}$–$\mathbf{L^3}$) molar ratio of 1 (Figures 5c-d, Supporting Information, Figures S11c-d and S12c-d; measured quantum yields, Φ, were 0.0022, 0.0027, 0.0032 for the 1:1 Zn^{2+} complexes with $\mathbf{L^1}$, $\mathbf{L^2}$, and $\mathbf{L^3}$, respectively). However, a smaller CHEF effect was also observed on adding Cd^{II} to all three ligands.

The comparison between the distribution curves derived from the potentiometric measurements and the pH dependence of the fluorescence emission at 380 nm for the Zn^{II}/**L** systems (Figure 6 for **L** = $\mathbf{L^2}$ and Supporting Information, Figure S13 for **L** = $\mathbf{L^1}$, $\mathbf{L^3}$) clearly indicates that the 1:1 species $[Zn(\mathbf{L})]^{2+}$ is responsible for the observed CHEF effect.[68] In H_2O (25 °C) solutions buffered at pH = 7.4 with MOPS, the optical responses of $\mathbf{L^1}$–$\mathbf{L^3}$ to the metal ions considered were very similar to those observed in MeCN/H_2O (1:1 v/v) solutions (Figure 7, Supporting Information, Figure S14), the only main

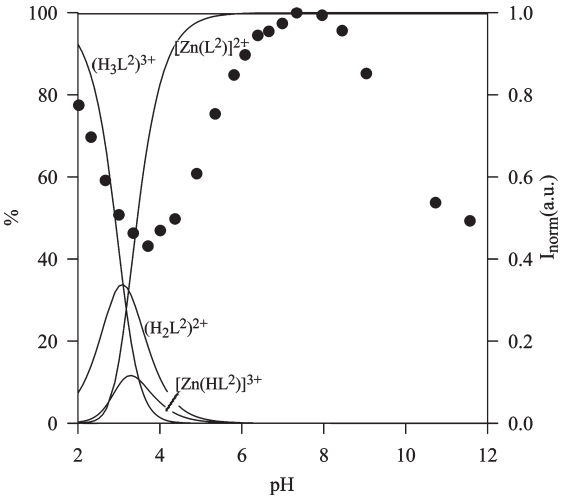

Figure 6. Distribution diagram for the system $Zn^{II}/\mathbf{L^2}$ in MeCN/H_2O (1:1 v/v, 0.10 M NMe_4Cl, 298.1 K $[Zn^{II}] = [\mathbf{L^2}] = 1 \times 10^{-3}$ M) and spectrofluorimetric data (●) from Supporting Information, Figure S10.

difference being the markedly lower CHEF effect in the presence of either Zn^{II} or Cd^{II} as compared to that observed in MeCN/H_2O (1:1 v/v, 25 °C), accompanied by a small decrease (less than a unit) in the $I_{rel}(Zn^{II})/I_{rel}(Cd^{II})$ ratio.

(68) The lack of perfect superimposition of the spectrofluorimetric curves to the distribution diagrams might be because the ionic media in the two types of experiments were different (Experimental Section).

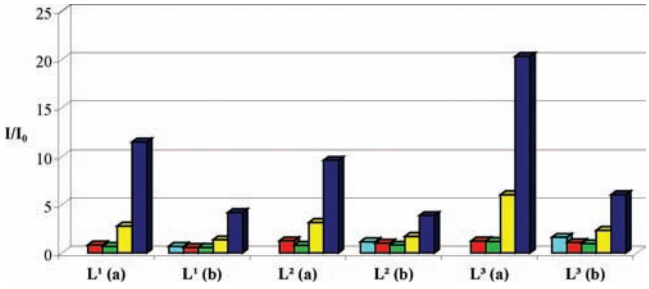

Figure 7. Effects [$I_{rel} = I/I_0$] on the fluorescence intensity of $\mathbf{L^1}-\mathbf{L^3}$ upon addition of Cu^{II} (green), Zn^{II} (blue), Cd^{II} (yellow), Hg^{II} (red), or Pb^{II} (cyan) [2 equiv, data taken from spectrofluorimetric titrations in Figures 5d, Supporting Information, Figures S11d and S12d] in MeCN/H_2O (1:1 v/v) (a), and H_2O (b) solutions buffered at pH = 7.4 with MOPS at 25 °C.

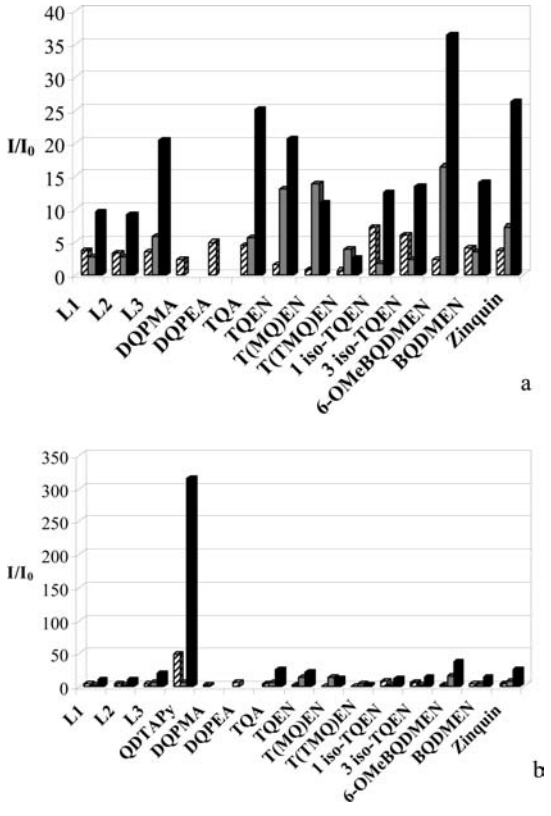

Figure 8. Relative fluorescence intensity [$I_{rel} = I/I_0$] of the ligands in Scheme 1 except **QDTAPy** (a), including **QDTAPy** (b), responding to 1 equiv of Zn^{II} (black bar) or Cd^{II} (gray bar), and the corresponding $I_{rel}(Zn^{II})/I_{rel}(Cd^{II})$ ratio (dashed bar). I_0 is the emission intensity of the ligands in the absence of metal ions: $\mathbf{L^1}-\mathbf{L^3}$ [MeCN/H_2O (1:1 v/v)]; **QDTAPy** [MeCN/H_2O (1:1 v/v)];[38] **DQPMA**, **DQPEA** (H_2O);[65] **TQA** [MeOH/H_2O (1:1 v/v)];[56] **TQEN**,[59] **T(MQ)EN**, **T(TMQ)EN**,[62] **1 iso-TQEN**, **3 iso-TQEN**,[64] **BQDMEN**, **6-OMeBQDMEN** [DMF/H_2O (1:1 v/v)];[67] **Zinquin** (H_2O).[66].

In Figure 8, the relative fluorescence intensity [$I_{rel} = I/I_0$] of the ligands in Scheme 1 responding to 1 equiv of Zn^{II} (black bar) or Cd^{II} (gray bar), and the corresponding $I_{rel}(Zn^{II})/I_{rel}(Cd^{II})$ ratios (dashed bar), are reported. Interestingly, despite data refer to different experimental conditions, all ligands showing a higher CHEF effect for Zn^{II} than for Cd^{II} (see Figure 8a) are characterized by a zinc(II) complex emission relative to cadmium(II) [$I_{rel}(Zn^{II})/I_{rel}(Cd^{II})$] ranging within a quite narrow interval from 7.19 (**1 iso-TQEN**) to 1.58 **TQEN**.[38,56,59,62,64−66] For Zinquin, the value of $I_{rel}(Zn^{II})/I_{rel}(Cd^{II})$ is 3.62, comparable to that observed for $\mathbf{L^1}-\mathbf{L^3}$.[66] Therefore, on going from a sterically crowded ligand such as **TQEN** to less sterically crowded ones such as **TQA** or **1 iso-TQEN** for which no significant $Zn-N_{(quinoline)}$ bond length distortions are observed in the corresponding Zn^{II}-complexes in the solid state, the $I_{rel}(Zn^{II})/I_{rel}(Cd^{II})$ ratio increases by a factor of 2.8 or 4.5, respectively.[56,59,64] This level of increase, while not negligible, is not outstanding either.

In our opinion, besides steric crowding effects other, more important additional factors need to be considered and investigated to fully understand the Zn^{II}/Cd^{II} discriminating ability of quinoline-based fluorescent chemosensors. In this respect, we are intrigued by the higher CHEF effect observed for Cd^{II} versus Zn^{II} with **T(MQ)EN**, where the 1:1 Zn^{II}-complex shows $Zn-N_{(quinoline)}$ bond length distortions comparable to those observed in the analogous complex with **TQEN** (Figure 8a).[59,62] Furthermore, with **QDTAPy** (Scheme 1) a $I_{rel}(Zn^{II})/I_{rel}(Cd^{II})$ ratio of about 50 is observed (Figure 8b),[38] despite the $Zn-N_{(quinoline)}$ bond distance in the complex $[Zn(\mathbf{QDTAPy})H_2O]^{2+}$ being comparable to those in the zinc(II) complexes with **TQA**, $\mathbf{L^1}-\mathbf{L^3}$, **1 iso-TQEN** and the other less sterically crowded quinoline-based ligands in Scheme 1.

Interestingly, as this manuscript was being finalized, the authors become aware of the online paper by Mikata et al.[69] on the fluorescence properties of the *bis*-quinoline derivatives **BQDMEN** and **6-OMeBQDMEN** (Scheme 1). Althought the $Zn-N_{(quinoline)}$ bond distances in [Zn(**BQDMEN**)Cl_2] are elongated [2.4362(15) Å] as compared to those in $[Zn(\mathbf{6\text{-}OMeBQDMEN})H_2O]^{2+}$ [2.113(3), 2.093(3) Å], the corresponding $I_{rel}(Zn^{II})/I_{rel}(Cd^{II})$ ratios are 4.0 and 2.2, respectively.

Conclusions

This manuscript describes the results achieved by a wide-ranging study concerned with the synthesis, coordination, and metal ion sensing properties of three new fluorescent quinoline pendant arm derivatives of [9]aneN_3 and [9]aneN_2S ($\mathbf{L^1}-\mathbf{L^3}$ in Scheme 1). In addition to the intrinsic interest in the coordination chemistry of the new three ligands, our results demonstrate that the ligands combine selective binding of Zn^{II} over Cd^{II} with discrimination in Zn^{II} sensing (the $I_{rel}(Zn^{II})/I_{rel}(Cd^{II})$ ratio is comparable to that observed for Zinquin). The stability of the Zn^{II}, Cd^{II}, and Pb^{II} complexes in solution seems to be mainly determined by a subtle balance between hydrophobic characteristics and steric crowding of ligands. In fact, selective binding of Zn^{II} over Cd^{II} and Pb^{II} is likely to be related to the greater degree of desolvation upon complexation of the smaller Zn^{II} cations with respect to the larger Cd^{II} and Pb^{II} ions. Furthermore, among the three ligands Zn^{II} forms the most stable complex with the less crowded ligand $\mathbf{L^2}$, which can impart stronger Zn−N coordination bonds thanks to its less rigid structure. Conversely, the study of the fluorescence emission properties of the complexes seems to suggest only a secondary role for steric effects in determining the ability of quinoline-based fluorescent chemosensors to discriminate between Zn^{II} and Cd^{II}.

(69) Mikata, Y.; Yamashita, A.; Kawamura, A.; Konno, H.; Miyamoto, Y.; Tamotsu, S. *Dalton Trans.* **2009**, 3800.

Acknowledgment. MIUR is gratefully acknowledged for financial support (Project PRIN 2007-C8RW53). We are grateful to EPSRC (U.K.) for support.

Supporting Information Available: Additional information as noted in the text and crystallographic data in CIF format [CCDC no. 733360−733369]. This material is available free of charge via the Internet at http://pubs.acs.org.